Synthesis and Modification of Gold Nanorods for Biomedical Applications

A thesis submitted in partial fulfillment for the degree of

Master of Science

as part of the

Integrated Ph.D. programme

(Materials Science)

by

Sonu. KP

Chemistry and Physics of Materials Unit

Jawaharlal Nehru Centre for Advanced Scientific Research

(Deemed University)

Bangalore, India

March 2014

Dedicated to My Mother

DECLARATION

I hereby declare that the matter embodied in the report entitled **"Synthesis and Modification of Gold Nanorods for Biomedical Applications"** is the result of investigations carried out by me at the Chemistry and Physics of Material Unit, Jawaharlal Nehru Centre for Advanced Scientific Research, under the supervision of Prof. Eswaramoorthy Muthusamy and that has not been submitted elsewhere for the award of any degree or diploma.

In keeping with the general practice in reporting scientific observations, due acknowledgement has been made whenever the work described is based on the findings of other investigators. Any omission that might have occurred due to oversight or error in the judgment is regretted.

Sonu.KP

CERTIFICATE

I hereby certify that the matter embodied in the report entitled **"Synthesis and Modification of Gold Nanorods for Biomedical Applications"** has been carried out by **Mr. Sonu. K P** under my supervision at Chemistry and Physics of Material Unit, Jawaharlal Nehru Centre for Advanced Scientific Research, Bangalore, India and that it has not been submitted elsewhere for the award of any degree or diploma.

Prof. Eswaramoorthy Muthusamy

ACKNOWLEDGEMENTS

I would like to take this opportunity to express a deep sense of gratitude to my thesis supervisor Prof. Eswaramoorthy Muthusamy, Chemistry and Physics of Material Unit, Jawaharlal Nehru Centre for Advanced Scientific Research. His competent guidance, stimulus, continuous encouragement and constructive criticism not only motivated me but also instilled a sense of confidence in me. The work presented in this project report would not have been accomplished without his unfailing attention and restless adherence to the finer scientific strictures. I would like thank him for introducing me to the fascinating world of nano materials.

I would like to thank Prof. C.N.R. Rao, FRS, for being a constant source of inspiration for me. I admire him for his enthusiastic inculcation of science.

I thank following faculties namely Prof. G.U. Kulkarni, Prof. S. Balasubramaniam, Prof. A. Sundaresan, Prof. K. S. Narayan, Prof. C. Narayana, Dr. T.K. Maji of CPMU, JNCASR, Prof. Swapan K. Pathi, Prof. Umesh V. Wagmare, Prof. S. Narasimhan, Dr. N.S. Vidhyadhiraja of TSU, JNCASR, Prof.S.M Shivaprasad of ICMS, JNCASR, Dr. Subi J. George, Prof. Ila, Dr. Jayanta Haldar for their courses.

I sincerely thank Dr. Subi J George with whom I worked on one of my problems. I also thank Mr. Mohit Kumar and Mr. Ankit Jain for helping me in carrying out the work.

I thank the timely help of the technical staff namely Ms. N. R. Selvi (for FESEM), Ms. T. Usha (for TEM), Mr. Vasu (for UV, PL, IR), Mr. Anil (for XRD), Mr. Mahesh (for SEM), Mr. Srinath, Mr. Srinivasa Rao and Mr. Srinivas (for technical assistance).

The service provided by JNCASR libraby, comlab, academics and administration were too critical and indispensible.

I also thank all my lab mates Mr. Piyush Chaturbedy, Mr. Pavan Kumar, Mr. Amritroop Achari, Mr. Sisir Maity, Mr. Dheeraj Kumar Singh. I thank my past lab mates Dr. K. K. R. Datta, Ms. Josena for their cooperation and company. I also acknowledge all the visiting scientists and students (POCE and SRF) for their company.

Cheer to all my Int. Ph.D. friends Mr. Abhijit Sen, Ms. Dipanwita Dutta, Mr. Rajib Sahu, Ms. Kandula Neelima, Mr. Uttam, Ms. Suchitra, Mr. Raaghesh for their enjoyable companionship. I would also like to thank all my friends specially Ms. Anamika, Mr. Arun Deepth, Mr. Jishnu, Mr. Vasudev, Ms. Priyanka, for cheerful moments. In the end, I would like to dedicate all the success to my mother whose sacrifices and struggles were the sole reason.

PREFACE

This thesis consists of three chapters. Chapter-1 introduces gold nanoparticles and signifies their applications for biomedical uses. Chapter-2 deals with fabrication of mesoporous silica coated gold nanorods and their application for anti-cancer drug delivery. Mesoporous silica coated gold nanorod flips its surface charge from negative to positive with pH which facilitates the delivery of anti-cancer drugs in cancer cells. Chapter 3 presents a novel strategy involving charge transfer module for the end-to-end assembly of the gold nanorods.

CONTENTS

Chapter-1

Introduction to Gold Nanoparticles

1.1 Introduction

Research on nanomaterials has recently drawn attention of world scientific community due its highly interdisciplinary nature.[1,2] The demand for the design of new nanomaterials and their self-assembled structures is ever interesting owing to their exciting properties[3-5].

Nanomaterials can be broadly classified into three categories, 0D, 1D and 2D depending on their dimensionalities.[6] For example, quantum dots, nanocrystals etc. fall into the category of zero-dimensional (0D); nanowires, nanorods etc. are one-dimensional (1D) and grapheme, thin films etc. are two-dimensional (2D) nanomaterials.

The high surface area and quantum confinement effects of nanomaterials make them useful for various applications in drug delivery[5,7,8], diagnostic applications[9-11], sensors and detectors[12-15], energy harvesting[16], photo-electronics[17], memory storage devices[18,19], catalysis[20] etc.

1.2 Noble Metal Nanoparticles

The story of metal nanoparticles started long time ago. Ancient civilizations produced and used metal nanoparticles for various applications utilizing their colour and medicinal properties.[21] One of the early and famous examples of metal nanoparticles used in ancient civilization is the Lycurgus Cup (Figure-1) which is presently preserved in British Museum.[22] The glass appears a deep wine-red colour in transmitted light while opaque green colour in reflected light due to the presence of gold nanoparticles in it.

The first documented scientific study of synthesis of metal nanoparticles was reported by Michael Faraday, who prepared gold nanocrystals by reducing aqueous solutions of chloroauric acid with phosphorous in presence of carbon disulfide.[23] In 1951, Turkevich described a new synthetic route for spherical gold nanoparticles with narrow size distribution using citrate as reducing agent in boiling aqueous solution of chloroauric acid.[24]

Figure-1: Lycurgus Cup (British Museum, AD 4th century). Colloidal gold cause a deep wine-red colour in transmitted light while opaque green colour in reflected light (Reprinted with permission from ref 22)

The advantage here is that citrate also serves as capping agent to prevent coagulation.[24,25] Later, Turkevich method was extended to synthesize other metal nanoparticles such as silver[26], palladium[27] etc.

Metal nanoparticles exhibit unique electronic, optical, photonic and catalytic properties owing to their size and shape.[28,29] The tremendous increase in the surface area per unit mass as a result of reduced dimensionality is one of the factors that alter the chemical and physical properties of the materials in nano regime. The large number of surface atoms and thus high surface energy determine the thermal stability and catalytic activity. Furthermore, the quantum confinement of electrons in the nanocrystals can also lead to novel optical, electronic and magnetic properties in nanoparticles. For example, bulk gold is a non-magnetic metal, whereas gold nanocrystals of size 2-4 nm exhibit excellent catalytic activity for various reactions[30] and they are magnetic in nature.[31]

1.3 Gold Nanoparticles

Among the noble metal nanoparticles, gold nanoparticles have been subjected to intense research for decades owing to their tunable electronic and optical properties.[32] Gold nanoparticles are widely used in biomedical applications due to their bio-compatibility[33], ease of surface functionalization[34] and promising optical properties.[35] Highly tunable optical properties of gold nanoparticles originate from the surface plasmon resonance (SPR).

1.3.1 Surface Plasmon resonance

Surface plasmon resonance (SPR) is an important phenomenon that makes metal nanoparticles unique.[36] Metals are generally treated as free-electron systems containing immobilized positive ions and free electrons. When a metal is irradiated with electromagnetic radiation, free electrons oscillate with a frequency, ω_p with respect to the positive ions. Quantized collective oscillation of the free electrons is called plasmon. The penetration depth for UV-vis-NIR radiations on metal surface is about few nanometers (for Au < 50nm).[37] Thus only surface electrons effectively interact with electromagnetic radiation and their collective oscillations are termed as surface plasmon. Figure-2 illustrates the interaction of metal nanoparticles with electromagnetic radiation.

The first mathematical model of the surface plasmon is given by Gustav Mie as solution of the classical Maxwell's equations for metal-dielectric interface.[38] Mie theory describes the light absorption of the spherical metal nanoparticles. The absorption spectra of metal nanospheres in a given solvent can be obtained using the optical constants of the bulk metal. According to Mie theory the absorption coefficient α ($mol^{-1}L\ cm^{-1}$) is given as follows.[39]

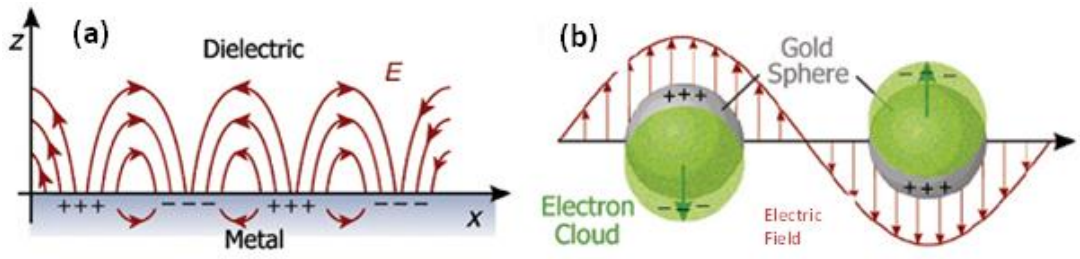

Figure-2: Schematic illustrations of collective oscillation of free electrons in (a) a metal-dielectric interface and (b) spherical gold nanoparticles. The electric field component of the incident light can collectively oscillate the free electrons from the lattice of positive ions. (Reprinted with permission from ref 37)

$$\alpha = \frac{18\pi}{ln10}\,\frac{10^5}{\lambda}\,\frac{Mn_0^3}{\rho}\,\frac{\varepsilon_2}{(\varepsilon_1 + 2n_0^2) + \varepsilon_2^2}$$

where M and ρ are molecular weight and density of the metal, λ is the wavelength of the incident light, n_0 is the refractive index of the solvent, ε_1 and ε_2 are real and imaginary part of the dielectric constant of the metal respectively. The imaginary part of the metal dielectric constant is given by the following relation for the particles smaller than the mean free path of the free electron.

$$\varepsilon_2 = \varepsilon_{2(bulk)} + \frac{\omega_p^2}{\omega^3}\,\frac{V_F}{R}$$

where ω_p is the plasmon frequency, ω is the frequency of the incident light, V_F is the velocity of electrons at Fermi level and R is the radius of spherical nanoparticles. Plasmon frequency can be described as follows.[37]

$$\omega_p = \frac{Ne^2}{m\varepsilon_0}$$

where *e* is charge on one electron, *N* is the concentration of free electrons in the metal, ε_o is the dielectric constant of the medium and *m is* the effective mass of an electron. The resonance of plasmon oscillation with incident light occurs when the ε_1 is twice the negative value of dielectric constant of medium. Gold nanoparticles are having plasmon absorption in visible - near IR region of the electromagnetic radiation.[40]

1.3.2 Size and shape dependence of surface plasmon resonance

Surface plasmon resonance is one of the important properties that highly depend upon the size of the metal nanoparticles. For example a red shift of up to 60 nm is observed in the absorption spectrum of spherical gold nanoparticles by increasing the diameter from 20 nm to 100 nm. Figure-3 shows the TEM images and absorption spectra of the spherical gold nanoparticles of various sizes.[41] Furthermore, gold nanoparticles show an additional intense peak in absorption spectrum when a shape anisotropy is introduced. Spherical gold nanoparticles show absorption peak at around 530 nm whereas rod shaped gold nanoparticles show two absorption peaks- one at around 530 nm and another in between 600 nm to 1400 nm depend on the aspect ratio of the gold rods. The 530 nm peak is typically due to the transverse plasmon oscillations while the other one at longer wavelength (600-1100 nm) is due the longitudinal oscillations.[42] Figure-4 shows the TEM images and absorption spectra of gold nanorods of various aspect ratios.[43]

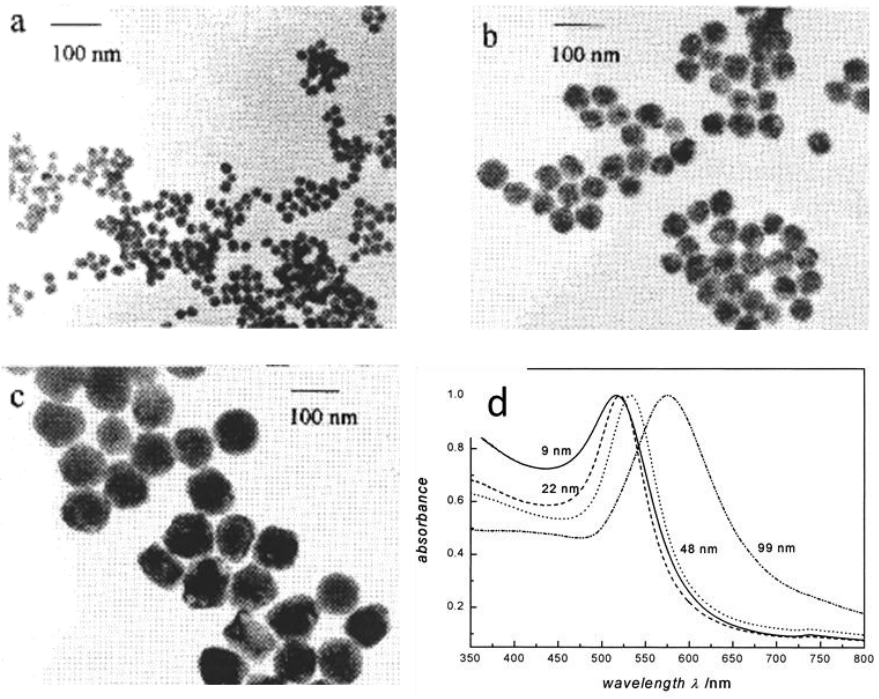

Figure-3: TEM images of the 22 (a), 48 (b), and 99 nm (c) gold nanoparticles and corresponding absorption spectra (d). (Reprinted with permission from ref 41)

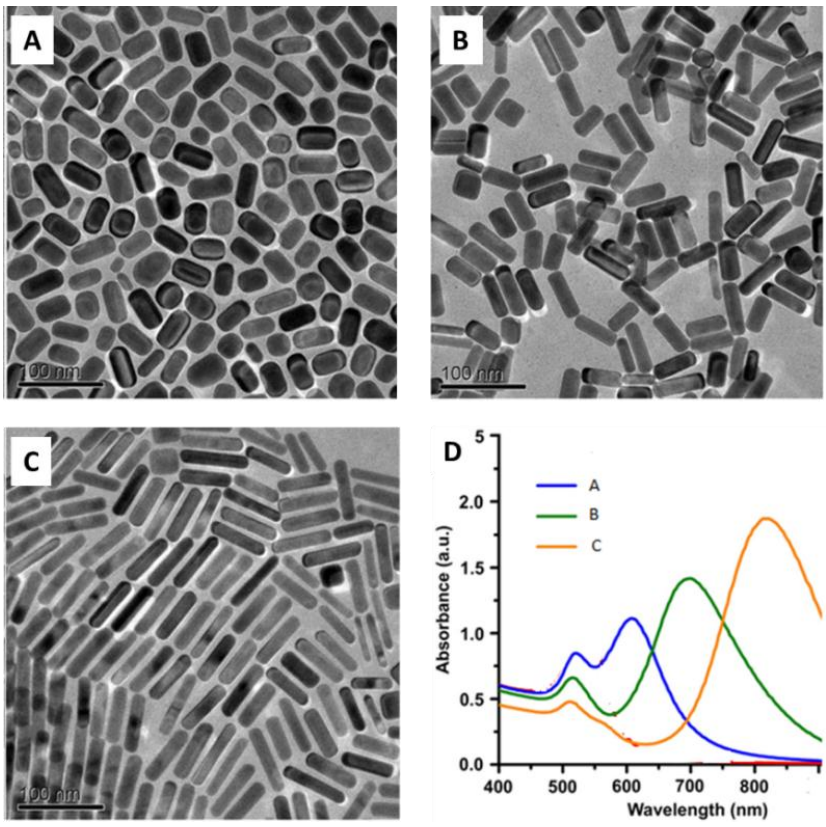

Figure-4: TEM images of the gold rods of the aspect ratio 1.9 (a), 2.9 (b), and 4.0 (c) and corresponding absorption spectra (d). (Reprinted with permission from ref 43)

1.3.3 Synthesis of gold nanoparticles

The methodologies developed to synthesize metal nanoparticles can be classified into "top-down"[44] and "bottom-up"[45] approaches and can be considered as physical and chemical methods respectively.

There have been a number of chemical methods developed for synthesis of gold nanorods such as hydrothermal synthesis[46], radiolytic reduction[47], chemical reduction[24], electrochemical reduction[48], photo-thermal reduction[49], biological synthesis[50] etc. Among them, chemical reduction of metal salts in aqueous and/or organic solvents, is the most common process.[51] Capping or stabilizing agents are important for this method, where they act as stabilizers against agglomeration of formed nanoparticles. The following methods are well-known for the synthesis of gold nanoparticles.

1.3.3.1 Turkevich method

It is the most popular method for obtaining spherical gold nanoparticles.[24] This method uses boiling citrate for reducing metal salt into nanoparticles. For example, spherical gold nanoparticles of size between 10 to 100 nm can be obtained by boiling aqueous solution of $HAuCl_4$ in presence of citrate.[25] Here citrate serves as both reducing agent and stabilizer. The particle size can be tuned by varying the concentration of reducing agent, metal precursor, additional halide ions etc.[24,52] For example, Figure-5 shows the TEM images of the spherical gold nanoparticles with various sizes prepared by varying chloride ion concentration.

1.3.3.2 Brust and Schiffrin method

It is a two phase method which is extensively used for synthesize of alkylthiol stabilized metal nanoparticles in organic medium. Tetraoctylammonium bromide (TOAB) is used as a phase transfer agent to transport metal precursor (for example, $HAuCl_4$) dissolved in water into toluene medium. The metal precursor is then reduced to nanoparticles by $NaBH_4$ in

toluene.[53] The particle size can be tuned between 1-30 nm range by changing experimental parameters.[54]

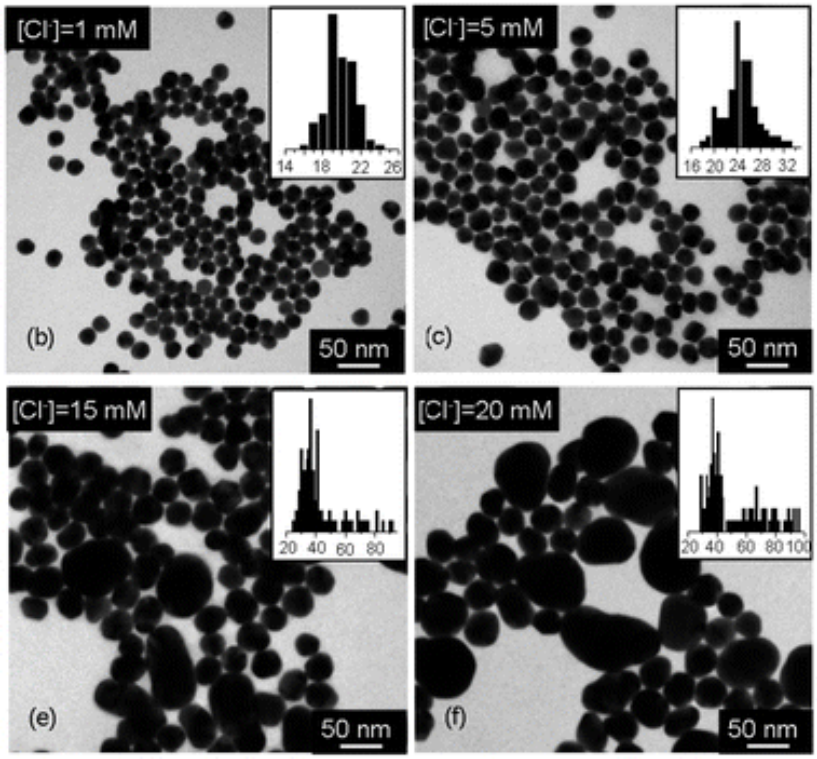

Figure-5: TEM images of the gold nanoparticles of various size synthesized by varying chloride ion concentration. (Reprinted with permission from ref 52)

1.3.3.3 Shape selective synthesis of gold nanoparticles

Wet chemical methods can be successfully employed to control the shape of the resulting metal nanoparticles.[55] One can obtain different shapes such as spheres[56], prisms[57], cubes[58], rods[59] etc. by controlling the experimental parameters like concentration of metal ions and/or stabilizers, pH, temperature, structure directing agents etc. For example, gold nanorods can be obtained from gold seed solution using mild reducing agent such as ascorbic acid or hydroquinone and cetyltrimethylammonium bromide (CTAB).[60,61] One can use silver ions to further control the shape of the rods.[62] Detailed mechanism of seed mediate growth of gold nanorods was proposed by Catherine J. Murphy *et al.*[62] Ascorbic acid being a mild reducing agent reduces Au^{3+} to Au^{+} and resulting $AuCl_2^-$ ions bind to CTAB micelles. The

collision between CTAB protected seed particles and micelles determine the rod like structure. Further, Ag^{+} is reduced to Ag^{0} and preferentially adsorb onto {110} facets of gold which inhibit the growth along that facet and lead to preferential growth of gold along {100} facet.[62] Figure-6 shows schematic of the growth mechanism.

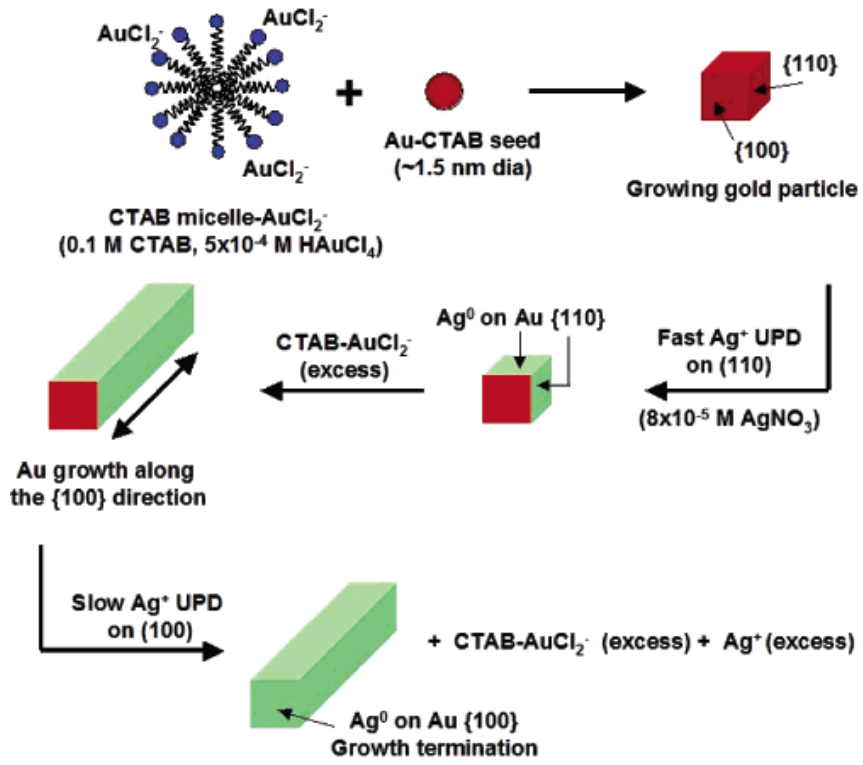

Figure-6: Schematic representation of the mechanism of nanorod growth from CTAB protected gold seed particles in the presence of Ag^{+}. (Reprinted with permission from ref 62)

1.4 Assembly of gold nanoparticles

In the last two decades, considerable improvement has been achieved in synthesis of gold nanoparticles of various size and shape. More recently, studies to achieve new properties by organizing or assembling individual nanoparticles have attracted considerable attraction.[21] The assembly of gold nanoparticles is important to understand the fundamentals of the properties arising from the collective behaviour of the individual nanoparticles. The collective behaviour has been used for various applications including sensing[12], nanocircuits[63], optical wave guiding[64], 'hot spot' generation[65] etc.

Major strategies for the assembly of metal nanoparticles involve point charge electrostatic attractions[66], hydrophobic interactions[67] etc. to drive the self-assembly; on the other hand external sources like electric field[68], magnetic field[42] etc. are also used to drive self-assembly. Bio-molecule assisted self-assembly is another exotic field which enables the bio-molecules recognition. For this antigen-antibody interaction[69], DNA base pairing[70] etc. are used. Self-assembled nanostructures have potential applications in sensors[71], bio-molecule recognition[72], optical filters[73], electronic devices[74] etc.

1.5 Applications of self-assembled gold nanoparticles

The collective behaviour of gold nanoparticles in self-assembled form has been used for various applications. The hot-spot formation at the junction of the gold nanoparticles in a self-assembly due to strong electromagnetic field is shown to have high raman enhancement compared to single particles.[75,76] This makes self-assembly of gold nanoparticles a useful tool in surface-enhanced raman scattering (SERS) experiments.

The assembly of the gold nanoparticles was successfully employed for sensing applications. For example, a simple colourimetric sensor for mercury ion detection based on gold nanoparticles assembly was reported, where DNA was used as a bio-linker to self-assemble the gold nanoparticles in presence of mercury ion.[77] The plasmonic shift was linearly related to the concentration of the mercury ion. Gold nanoparticle self-assembly is also used for the detection of biomolecules like Cysteine, Glutathione etc.[66]

1.6 Bio-medical applications of gold nanoparticles

The interaction of nanoparticles with biological system has great potentials.[35] Gold nanoparticles are important in biology owing to their relative non-toxic nature.[35] This makes them suitable for drug delivery and imaging platforms. Time, size and shape dependent bio-distribution and elimination of gold nanoparticles are useful for non-targeted delivery.[78] Gold nanoparticle surface chemistry can also be engineered to alter the bio-distribution. Gold

nanoparticles are also well exploited for highly sensitive diagnosis assays[79] and thermal ablation.[80]

1.6.1 Anti-cancer drug delivery systems

Cancer is one of the leading causes of mortality in the modern world. Gold nanoparticles are highly promising candidates to fight against cancer owing to their unique biological interactions.[81] Considerable amount of reports describing various constructions of anti-cancer drug delivery systems based on gold nanoparticles are present.[82-84] Specific accumulation and delivery of drugs at cancer sites are the added advantages in these drug delivery systems. The accumulation can be through passive means as well as through active means.[85] Passive accumulation is mediated through Enhanced Permeation Retention effect (EPR effect).[86] Extensive angiogenesis happening at the cancer site due to overexpressed VEGF (Vascular endothelial growth factor) leads to the immature leaky capillaries at cancer tissue, which help immobilization of nanoparticles at the cancer tissue (EPR effect).[87] Active immobilization involves surface modification to alter the bio-distribution of the nanoparticles.[88] Ease of surface functionalization of gold nanoparticles through Au-S strong covalent bond makes them promising materials as an active targeting platform. Acidic nature of the cancerous tissue is extensively used to target nanoparticles into cancer sites by functionalizing the surface of the nanoparticles with pH responsive moieties[83]. Further, specific interactions such as enzyme-substrate binding[89], antibody- antigen interactions[90] etc. are also used to target nanoparticles to cancer sites.

1.6.2 Photo thermal therapy

Combination therapy is another popular way to fight against cancer using the gold nanoparticles, where surface plasmon resonance is used along with anti-cancer drugs to kill cancer cells.[91] Gold nanorods are well known for the SPR assisted therapy or photo thermal destruction owing to their near IR longitudinal plasmon peak and high absorption cross

section.[89] Once accumulated, gold nanorods can convert the IR radiation into thermal energy and locally heat the cancer tissue.[92] Under normal biological dose gold nanorods can increase the temperature up to 50 ^{0}C which leads the cancer cells to die.[93] Apart from photo thermal therapy gold nanorods can also be used for IR imaging[94] and CT contrasting.[95]

1.7 Conclusion

Gold nanoparticles are an important class of nanomaterials. Fine control over the size and shape selective synthesis of gold nanoparticles enables exploration and manipulation of various properties. Gold nanoparticles are successfully applied to various traditional disciplines such as sensing, bio-imaging, diagnostics, therapeutics etc. which revolutionize the existing scenario. Among others, cancer diagnosis and therapy is one important application of gold nanoparticles. In spite of the advances in synthesis and design of nanoparticle based bio-medical platforms, combining various diagnosis and therapeutic tools into single system is yet a challenge to be addressed. The collective behaviour of gold nanoparticles in self-assembled nanostructures has been explored for various applications such as sensing, surface enhanced raman spectroscopy etc. Precise control over self-assembly is important for the applications of self-assembled gold nanoparticles. Among several strategies for the assembly of gold nanoparticles, a supramolecular approach is less explored in spite of its advantages.

1.8 References

1 Sanchez, C., Belleville, P., Popall, M. & Nicole, L. Applications of advanced hybrid organic-inorganic nanomaterials: from laboratory to market. *Chem. Soc. Rev.* **40**, 696-753, (2011).

2 Arico, A. S., Bruce, P., Scrosati, B., Tarascon, J.-M. & van Schalkwijk, W. Nanostructured materials for advanced energy conversion and storage devices. *Nat Mater* **4**, 366-377, (2005).

3 Mann, S. Self-assembly and transformation of hybrid nano-objects and nanostructures under equilibrium and non-equilibrium conditions. *Nat Mater* **8**, 781-792, (2009).

4 Sanchez, C., Arribart, H. & Giraud Guille, M. M. Biomimetism and bioinspiration as tools for the design of innovative materials and systems. *Nat Mater* **4**, 277-288, (2005).

5 Mitragotri, S. & Lahann, J. Physical approaches to biomaterial design. *Nat Mater* **8**, 15-23, (2009).

6 Rao, C. N. R. & Cheetham, A. K. Science and technology of nanomaterials: current status and future prospects. *J. Mater. Chem.* **11**, 2887-2894, (2001).

7 Irvine, D. J. Drug delivery: One nanoparticle, one kill. *Nat Mater* **10**, 342-343, (2011).

8 Putnam, D. Drug delivery: The heart of the matter. *Nat Mater* **7**, 836-837, (2008).

9 Hubbell, J. A. & Langer, R. Translating materials design to the clinic. *Nat Mater* **12**, 963-966, (2013).

10 Eaton, M. Nanomedicine: Industry-wise research. *Nat Mater* **6**, 251-253, (2007).

11 Xia, Y. Nanomaterials at work in biomedical research. *Nat Mater* **7**, 758-760, (2008).

12 Anker, J. N., Hall, W. P., Lyandres, O., Shah, N. C., Zhao, J. & Van Duyne, R. P. Biosensing with plasmonic nanosensors. *Nat Mater* **7**, 442-453, (2008).

13 Kabashin, A. V., Evans, P., Pastkovsky, S., Hendren, W., Wurtz, G. A., Atkinson, R., Pollard, R., Podolskiy, V. A. & Zayats, A. V. Plasmonic nanorod metamaterials for biosensing. *Nat Mater* **8**, 867-871, (2009).

14 Wei, H. & Wang, E. Nanomaterials with enzyme-like characteristics (nanozymes): next-generation artificial enzymes. *Chem. Soc. Rev.* **42**, 6060-6093, (2013).

15 Rurack, K. Nanoparticle-based sensors: Striped cation-trappers. *Nat Mater* **11**, 913-914, (2012).

16 Kamat, P. V. Meeting the Clean Energy Demand: Nanostructure Architectures for Solar Energy Conversion. *J. Phys. Chem. C* **111**, 2834-2860, (2007).

17 Zheludev, N. I. & Kivshar, Y. S. From metamaterials to metadevices. *Nat Mater* **11**, 917-924, (2012).

18 Chappert, C., Fert, A. & Van Dau, F. N. The emergence of spin electronics in data storage. *Nat Mater* **6**, 813-823, (2007).

19 Wuttig, M. & Yamada, N. Phase-change materials for rewriteable data storage. *Nat Mater* **6**, 824-832, (2007).

20 Zaera, F. Nanostructured materials for applications in heterogeneous catalysis. *Chem. Soc. Rev.* **42**, 2746-2762, (2013).

21 Daniel, M.-C. & Astruc, D. Gold Nanoparticles: Assembly, Supramolecular Chemistry, Quantum-Size-Related Properties, and Applications toward Biology, Catalysis, and Nanotechnology. *Chem. Rev.* **104**, 293-346, (2003).

22 Wagner, F. E., Haslbeck, S., Stievano, L., Calogero, S., Pankhurst, Q. A. & Martinek, K. P. Before striking gold in gold-ruby glass. *Nature* **407**, 691-692, (2000).

23 Faraday, M. The Bakerian Lecture: Experimental Relations of Gold (and Other Metals) to Light. *Philos. Trans. R. Soc. London* **147**, 145-181, (1857).

24 Kimling, J., Maier, M., Okenve, B., Kotaidis, V., Ballot, H. & Plech, A. Turkevich Method for Gold Nanoparticle Synthesis Revisited. *J. Phys. Chem. B* **110**, 15700-15707, (2006).

25 Turkevich, J., Stevenson, P. C. & Hillier, J. A study of the nucleation and growth processes in the synthesis of colloidal gold. *Discuss.Faraday Soc.* **11**, 55-75, (1951).

26 Pillai, Z. S. & Kamat, P. V. What Factors Control the Size and Shape of Silver Nanoparticles in the Citrate Ion Reduction Method? *J. Phys. Chem. B* **108**, 945-951, (2003).

27 Kim, J.-H., Chung, H.-W. & Lee, T. R. Preparation and Characterization of Palladium Shells with Gold and Silica Cores. *Chem. Mater.* **18**, 4115-4120, (2006).

28 Kelly, K. L., Coronado, E., Zhao, L. L. & Schatz, G. C. The Optical Properties of Metal Nanoparticles: The Influence of Size, Shape, and Dielectric Environment. *J. Phys. Chem. B* **107**, 668-677, (2002).

29 El-Sayed, M. A. Some Interesting Properties of Metals Confined in Time and Nanometer Space of Different Shapes. *Acc. Chem. Res.* **34**, 257-264, (2001).

30 Lopez, N., Janssens, T. V. W., Clausen, B. S., Xu, Y., Mavrikakis, M., Bligaard, T. & Nørskov, J. K. On the origin of the catalytic activity of gold nanoparticles for low-temperature CO oxidation. *J. Catal.* **223**, 232-235, (2004).

31 Crespo, P., Litrán, R., Rojas, T. C., Multigner, M., de la Fuente, J. M., Sánchez-López, J. C., García, M. A., Hernando, A., Penadés, S. & Fernández, A. Permanent Magnetism, Magnetic Anisotropy, and Hysteresis of Thiol-Capped Gold Nanoparticles. *Phys. Rev. Lett.* **93**, 087204, (2004).

32 Huang, X., Jain, P. K., El-Sayed, I. H. & El-Sayed, M. A. Gold nanoparticles: interesting optical properties and recent applications in cancer diagnostics and therapy. *Nanomedicine* **2**, 681-693, (2007).

33 Boisselier, E. & Astruc, D. Gold nanoparticles in nanomedicine: preparations, imaging, diagnostics, therapies and toxicity. *Chem. Soc. Rev.* **38**, 1759-1782, (2009).

34 Gao, J., Huang, X., Liu, H., Zan, F. & Ren, J. Colloidal Stability of Gold Nanoparticles Modified with Thiol Compounds: Bioconjugation and Application in Cancer Cell Imaging. *Langmuir* **28**, 4464-4471, (2012).

35 Murphy, C. J., Gole, A. M., Stone, J. W., Sisco, P. N., Alkilany, A. M., Goldsmith, E. C. & Baxter, S. C. Gold Nanoparticles in Biology: Beyond Toxicity to Cellular Imaging. *Acc. Chem. Res.* **41**, 1721-1730, (2008).

36 Mayer, K. M. & Hafner, J. H. Localized Surface Plasmon Resonance Sensors. *Chem. Rev.* **111**, 3828-3857, (2011).

37 Xia, Y. & Halas, N. J. Shape-Controlled Synthesis and Surface Plasmonic Properties of Metallic Nanostructures. *MRS Bull.* **30**, 338-348, (2005).

38 Link, S. & El-Sayed, M. A. Shape and size dependence of radiative, non-radiative and photothermal properties of gold nanocrystals. *Int. Rev. Phys. Chem.* **19**, 409-453, (2000).

39 Link, S. & El-Sayed, M. A. Optical properties and ultrafast dynamics of metallic nanocrystals. *Annu Rev Phys Chem* **54**, 331-366, (2003).

40 Jain, P. K., Huang, X., El-Sayed, I. H. & El-Sayed, M. A. Noble Metals on the Nanoscale: Optical and Photothermal Properties and Some Applications in Imaging, Sensing, Biology, and Medicine. *Acc. Chem. Res.* **41**, 1578-1586, (2008).

41 Link, S. & El-Sayed, M. A. Size and Temperature Dependence of the Plasmon Absorption of Colloidal Gold Nanoparticles. *J. Phys. Chem. B* **103**, 4212-4217, (1999).

42 Wang, M., Gao, C., He, L., Lu, Q., Zhang, J., Tang, C., Zorba, S. & Yin, Y. Magnetic Tuning of Plasmonic Excitation of Gold Nanorods. *J. Am. Chem. Soc.* **135**, 15302-15305, (2013).

43 Qiu, Y., Liu, Y., Wang, L., Xu, L., Bai, R., Ji, Y., Wu, X., Zhao, Y., Li, Y. & Chen, C. Surface chemistry and aspect ratio mediated cellular uptake of Au nanorods. *Biomaterials* **31**, 7606-7619, (2010).

44 Eustis, S. & El-Sayed, M. A. Why gold nanoparticles are more precious than pretty gold: Noble metal surface plasmon resonance and its enhancement of the radiative and nonradiative properties of nanocrystals of different shapes. *Chem. Soc. Rev.* **35**, 209-217, (2006).

45 Cushing, B. L., Kolesnichenko, V. L. & O'Connor, C. J. Recent Advances in the Liquid-Phase Syntheses of Inorganic Nanoparticles. *Chem. Rev.* **104**, 3893-3946, (2004).

46 Tang, X.-L., Jiang, P., Ge, G.-L., Tsuji, M., Xie, S.-S. & Guo, Y.-J. Poly(N-vinyl-2-pyrrolidone) (PVP)-Capped Dendritic Gold Nanoparticles by a One-Step Hydrothermal Route and Their High SERS Effect. *Langmuir* **24**, 1763-1768, (2008).

47 Henglein, A. & Meisel, D. Radiolytic Control of the Size of Colloidal Gold Nanoparticles. *Langmuir* **14**, 7392-7396, (1998).

48 Rodríguez-Sánchez, L., Blanco, M. C. & López-Quintela, M. A. Electrochemical Synthesis of Silver Nanoparticles. *J. Phys. Chem. B* **104**, 9683-9688, (2000).

49 Lu, W.-E., Zheng, M.-L., Chen, W.-Q., Zhao, Z.-S. & Duan, X.-M. Gold nanoparticles prepared by glycinate ionic liquid assisted multi-photon photoreduction. *Phys. Chem. Chem. Phys.* **14**, 11930-11936, (2012).

50 Thakkar, K. N., Mhatre, S. S. & Parikh, R. Y. Biological synthesis of metallic nanoparticles. *Nanomedicine*. **6**, 257-262, (2010).

51 Park, J., Joo, J., Kwon, S. G., Jang, Y. & Hyeon, T. Synthesis of Monodisperse Spherical Nanocrystals. *Angew. Chem. Int. Ed.* **46**, 4630-4660, (2007).

52 Zhao, L., Jiang, D., Cai, Y., Ji, X., Xie, R. & Yang, W. Tuning the size of gold nanoparticles in the citrate reduction by chloride ions. *Nanoscale* **4**, 5071-5076, (2012).

53 Jin, R. Quantum sized, thiolate-protected gold nanoclusters. *Nanoscale* **2**, 343-362, (2010).

54 Liz-Marzan, L. M. Gold nanoparticle research before and after the Brust-Schiffrin method. *Chem. Commun.* **49**, 16-18, (2013).

55 Zhi-Chuan, X., Cheng-Min, S., Cong-Wen, X., Tian-Zhong, Y., Huai-Ruo, Z., Jian-Qi, L., Hu-Lin, L. & Hong-Jun, G. Wet chemical synthesis of gold nanoparticles using silver seeds: a shape control from nanorods to hollow spherical nanoparticles. *Nanotechnology* **18**, 115608, (2007).

56 Perrault, S. D. & Chan, W. C. W. Synthesis and Surface Modification of Highly Monodispersed, Spherical Gold Nanoparticles of 50−200 nm. *J. Am. Chem. Soc.* **131**, 17042-17043, (2009).

57 Pastoriza-Santos, I. & Liz-Marzán, L. M. Synthesis of Silver Nanoprisms in DMF. *Nano Lett.* **2**, 903-905, (2002).

58 Sun, Y. & Xia, Y. Shape-Controlled Synthesis of Gold and Silver Nanoparticles. *Science* **298**, 2176-2179, (2002).

59 Xia, Y., Xiong, Y., Lim, B. & Skrabalak, S. E. Shape-Controlled Synthesis of Metal Nanocrystals: Simple Chemistry Meets Complex Physics? *Angew. Chem. Int. Ed.* **48**, 60-103, (2009).

60 Nikoobakht, B. & El-Sayed, M. A. Preparation and Growth Mechanism of Gold Nanorods (NRs) Using Seed-Mediated Growth Method. *Chem. Mater.* **15**, 1957-1962, (2003).

61 Vigderman, L. & Zubarev, E. R. High-Yield Synthesis of Gold Nanorods with Longitudinal SPR Peak Greater than 1200 nm Using Hydroquinone as a Reducing Agent. *Chem. Mater.* **25**, 1450-1457, (2013).

62 Orendorff, C. J. & Murphy, C. J. Quantitation of Metal Content in the Silver-Assisted Growth of Gold Nanorods. *J. Phys. Chem. B* **110**, 3990-3994, (2006).

63 Ozbay, E. Plasmonics: Merging Photonics and Electronics at Nanoscale Dimensions. *Science* **311**, 189-193, (2006).

64 Maier, S. A., Kik, P. G., Atwater, H. A., Meltzer, S., Harel, E., Koel, B. E. & Requicha, A. A. G. Local detection of electromagnetic energy transport below the diffraction limit in metal nanoparticle plasmon waveguides. *Nat Mater* **2**, 229-232, (2003).

65 Lee, A., Andrade, G. F. S., Ahmed, A., Souza, M. L., Coombs, N., Tumarkin, E., Liu, K., Gordon, R., Brolo, A. G. & Kumacheva, E. Probing Dynamic Generation of Hot-Spots in Self-Assembled Chains of Gold Nanorods by Surface-Enhanced Raman Scattering. *J. Am. Chem. Soc.* **133**, 7563-7570, (2011).

66 Sudeep, P. K., Joseph, S. T. S. & Thomas, K. G. Selective Detection of Cysteine and Glutathione Using Gold Nanorods. *J. Am. Chem. Soc.* **127**, 6516-6517, (2005).

67 Nie, Fava, D., Rubinstein, M. & Kumacheva, E. "Supramolecular" Assembly of Gold Nanorods End-Terminated with Polymer "Pom-Poms": Effect of Pom-Pom Structure on the Association Modes. *J. Am. Chem. Soc.* **130**, 3683-3689, (2008).

68 Pescaglini, A., Emanuele, U., Riordan, A. O. & Daniela, I. Dielectrophoretic Self-Assembly of Au Nanorods for Sensing Applications. *Journal of Physics: Conference Series* **307**, 012051, (2011).

69 Shenton, W., Davis, S. A. & Mann, S. Directed Self-Assembly of Nanoparticles into Macroscopic Materials Using Antibody–Antigen Recognition. *Adv. Mater.* **11**, 449-452, (1999).

70 Krpetić, Ž., Singh, I., Su, W., Guerrini, L., Faulds, K., Burley, G. A. & Graham, D. Directed Assembly of DNA-Functionalized Gold Nanoparticles Using Pyrrole–Imidazole Polyamides. *J. Am. Chem. Soc.* **134**, 8356-8359, (2012).

71 Cheng, S. F. & Chau, L. K. Colloidal gold-modified optical fiber for chemical and biochemical sensing. *Anal Chem* **75**, 16-21, (2003).

72 Maxwell, D. J., Taylor, J. R. & Nie, S. Self-Assembled Nanoparticle Probes for Recognition and Detection of Biomolecules. *J. Am. Chem. Soc.* **124**, 9606-9612, (2002).

73 Dirix, Y., Bastiaansen, C., Caseri, W. & Smith, P. Oriented Pearl-Necklace Arrays of Metallic Nanoparticles in Polymers: A New Route Toward Polarization-Dependent Color Filters. *Adv. Mater.* **11**, 223-227, (1999).

74 Leroux, Y., Lacroix, J. C., Fave, C., Stockhausen, V., Félidj, N., Grand, J., Hohenau, A. & Krenn, J. R. Active Plasmonic Devices with Anisotropic Optical Response: A Step Toward Active Polarizer. *Nano Lett.* **9**, 2144-2148, (2009).

75 Orendorff, C. J., Gearheart, L., Jana, N. R. & Murphy, C. J. Aspect ratio dependence on surface enhanced Raman scattering using silver and gold nanorod substrates. *Phys. Chem. Chem. Phys.* **8**, 165-170, (2006).

76 Zhu, Z., Meng, H., Liu, W., Liu, X., Gong, J., Qiu, X., Jiang, L., Wang, D. & Tang, Z. Superstructures and SERS Properties of Gold Nanocrystals with Different Shapes. *Angew. Chem.* **123**, 1631-1634, (2011).

77 Wang, Y., Li, Y. F., Wang, J., Sang, Y. & Huang, C. Z. End-to-end assembly of gold nanorods by means of oligonucleotide-mercury(ii) molecular recognition. *Chem. Commun.* **46**, 1332-1334, (2010).

78 Sonavane, G., Tomoda, K. & Makino, K. Biodistribution of colloidal gold nanoparticles after intravenous administration: Effect of particle size. *Colloids Surf B Biointerfaces* **66**, 274-280, (2008).

79 Lu, F., Doane, T. L., Zhu, J.-J. & Burda, C. Gold nanoparticles for diagnostic sensing and therapy. *Inorganica Chimica Acta* **393**, 142-153, (2012).

80 Cardinal, J., Klune, J. R., Chory, E., Jeyabalan, G., Kanzius, J. S., Nalesnik, M. & Geller, D. A. Noninvasive radiofrequency ablation of cancer targeted by gold nanoparticles. *Surgery* **144**, 125-132, (2008).

81 Jain, S., Hirst, D. G. & O'Sullivan, J. M. Gold nanoparticles as novel agents for cancer therapy. *British Journal of Radiology* **85**, 101-113, (2012).

82 Brown, S. D., Nativo, P., Smith, J.-A., Stirling, D., Edwards, P. R., Venugopal, B., Flint, D. J., Plumb, J. A., Graham, D. & Wheate, N. J. Gold Nanoparticles for the Improved Anticancer Drug Delivery of the Active Component of Oxaliplatin. *J. Am. Chem. Soc.* **132**, 4678-4684, (2010).

83 Ghosh, P., Han, G., De, M., Kim, C. K. & Rotello, V. M. Gold nanoparticles in delivery applications. *Adv. Drug Deliv. Rev.* **60**, 1307-1315, (2008).

84 Han, G., Ghosh, P. & Rotello, V. M. Functionalized gold nanoparticles for drug delivery. *Nanomedicine* **2**, 113-123, (2007).

85 Byrne, J. D., Betancourt, T. & Brannon-Peppas, L. Active targeting schemes for nanoparticle systems in cancer therapeutics. *Adv. Drug Deliv. Rev.* **60**, 1615-1626, (2008).

86 Maeda, H., Sawa, T. & Konno, T. Mechanism of tumor-targeted delivery of macromolecular drugs, including the EPR effect in solid tumor and clinical overview of the prototype polymeric drug SMANCS. *J. Controlled Release* **74**, 47-61, (2001).

87 Maeda, H., Fang, J., Inutsuka, T. & Kitamoto, Y. Vascular permeability enhancement in solid tumor: various factors, mechanisms involved and its implications. *International Immunopharmacology* **3**, 319-328, (2003).

88 Khlebtsov, N. & Dykman, L. Biodistribution and toxicity of engineered gold nanoparticles: a review of in vitro and in vivo studies. *Chem. Soc. Rev.* **40**, 1647-1671, (2011).

89 Koivunen, E., Arap, W., Valtanen, H., Rainisalo, A., Medina, O. P., Heikkila, P., Kantor, C., Gahmberg, C. G., Salo, T., Konttinen, Y. T., Sorsa, T., Ruoslahti, E. & Pasqualini, R. Tumor targeting with a selective gelatinase inhibitor. *Nat Biotech* **17**, 768-774, (1999).

90 Gao, X., Cui, Y., Levenson, R. M., Chung, L. W. K. & Nie, S. In vivo cancer targeting and imaging with semiconductor quantum dots. *Nat Biotech* **22**, 969-976, (2004).

91 Ren, F., Bhana, S., Norman, D. D., Johnson, J., Xu, L., Baker, D. L., Parrill, A. L. & Huang, X. Gold Nanorods Carrying Paclitaxel for Photothermal-Chemotherapy of Cancer. *Bioconjugate Chemistry* **24**, 376-386, (2013).

92 Huff, T. B., Tong, L., Zhao, Y., Hansen, M. N., Cheng, J.-X. & Wei, A. Hyperthermic effects of gold nanorods on tumor cells. *Nanomedicine* **2**, 125-132, (2007).

93 Yang, X., Liu, X., Liu, Z., Pu, F., Ren, J. & Qu, X. Near-Infrared Light-Triggered, Targeted Drug Delivery to Cancer Cells by Aptamer Gated Nanovehicles. *Adv. Mater.* **24**, 2890-2895, (2012).

94 Huang, X., El-Sayed, I. H., Qian, W. & El-Sayed, M. A. Cancer Cell Imaging and Photothermal Therapy in the Near-Infrared Region by Using Gold Nanorods. *J. Am. Chem. Soc.* **128**, 2115-2120, (2006).

95 Xi, D., Dong, S., Meng, X., Lu, Q., Meng, L. & Ye, J. Gold nanoparticles as computerized tomography (CT) contrast agents. *RSC Advances* **2**, 12515-12524, (2012).

Chapter-2

Mesoporous silica coated gold nanorods: Optimization for Efficient Anticancer Drug Delivery

Summary:

This chapter discusses design, synthesis and application of mesoporous silica coated gold nanorods as an efficient anticancer drug delivery platform. Considering the acidic nature of cancer extracellular fluid, the drug delivery system is designed to flip the surface charge from negative to positive at acidic pH which facilitate the release of positively charged drug and hence drug delivery to the cancer cells. Promising drug release is shown by our system in endosomal pH of 5.

2.1 Introduction:

Cancer is still one of the major causes of death, despite decades of intense research and development of novel chemotherapeutics and diagnostics.[1-3] Nanomaterials based drug delivery systems (DDS) are emerging as an important class of therapeutics in recent years owing to their modifiable pharmacokinetics and pharmacodynamics.[4-7]

To improve the therapeutic effects of anticancer drugs, active as well as passive targeting methods[8,9] were employed. Active targeting involves incorporation of biologically active molecules into the drug delivery systems which specifically bind to the enzymes over expressed on the cancer cells.[10,11] On the other hand, passive targeting does not involve any biological active molecules.[12] Passive targeting has been largely explored for anticancer drug delivery using a simple pharmacokinetic mechanism known as Enhanced Permeation and Retention (EPR) effect[13-15] which is enhanced accumulation in the cancerous extracellular matrix through leaky blood vessels at the cancer site. These leaky blood vessels are the result of abnormal angiogenesis occurs at cancerous extracellular matrix due to upregulated vascular endothelial growth factor (VGEF) and other signaling pathways. It is through these leaky blood vessels the drug delivery systems tend to accumulate in the cancerous extracellular matrix[14], and therefore the accumulation through EPR effect depends on the size of the particles.[4,16] This enables us to design delivery systems of desired bio-distribution, pharmacokinetics and pharmacodynamics. Figure-1 shows a schematic representation of EPR effect.

To further improve the spatial control of drug delivery, many smart systems have been developed which are typically stimuli responsive in nature.[17,18] Various stimuli such as pH[19-22], temperature[19,23], specific chemical reactions[24], enzymes[25] etc. have been incorporated. Due to the upregulated synthesis of lactic acid in the cancer cells, the extracellular matrix is slightly acidic. For this reason, pH based stimulus have been highly explored for anticancer drug delivery.

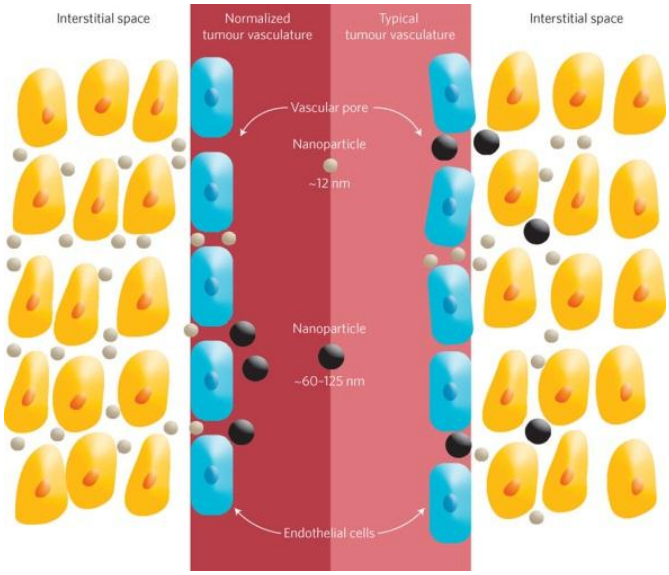

Figure-1: Schematic representation of EPR effect (Reprinted with permission from ref 16).

To control drug delivery systems remotely and temporally, it is advantageous to use external non-invasive stimuli such as light[26], magnetic field[27] and electric field[28] etc. Among them light has been shown as promising stimulus for further clinical uses.[29] However, the systems which use UV light to excite photosensitizers are found to be less attractive because of UV radiation's limited penetration depth in tissues due to quick attenuation[30]. Therefore, it is desirable to use NIR radiation as an external stimulus owing to its high penetration depth and biocompatibility.[31,32] Photodynamic therapy is another interesting application of the NIR radiation in cancer treatment which involves local temperature elevation at cancer site that leads to the destruction of cancer cells.[33]

Gold nanorods (AuNRs) are important in this regard because of their NIR absorption due to longitudinal plasmon resonance which can be tuned across the NIR window (700 nm to 1500 nm) with respect to the aspect ratio.[34] Owing to the high absorption coefficient, gold nanorods can convert NIR radiation to heat rapidly and hence find use as hyperthermia agents for the treatment of cancer. [35,36] However, well known seed mediated synthesis uses CTAB

(Cetyl trimethylammonium bromide) as capping agent which is highly cytotoxic; therefore, it is necessary to modify the surface of the gold nanorods.[37] Various surface modifications of gold nanorods using polyethylene[38], polyelectrolyte[39] and silica coating[40,41] were reported in the literature. Among these, mesoporous silica coating is important owing to its high payload capacity[42,43], good biocompatibility[44] and facile surface modifiability.[45]

Mesoporous silica coated gold nanorods provide a multi-functional platform for combination therapy where physical ablation and chemotherapy are used simultaneously for achieving maximum therapeutic effect.[46,47] Gold core can be used for the imaging and hyperthermia, whereas mesoporous silica can act as an anticancer drug carrier. These multi-functional materials are important milestones in the way towards personalized medicine.[48-50]

2.2 Scope of the present study:

Though EPR effect allows effective localization of drug delivery systems in cancerous extra cellular matrix, immobilization inside the cell is more important and challenging.[51,52] Delivery of anti-cancer drugs to the extracellular matrix is less efficient because several of them are lipid bilayer impermeable.[53,54] To overcome this issue, various drug delivery systems were designed to utilize active targeting for the cellular internalization that involve specific biochemical interactions.[55] Recently Jun Wang et al., demonstrated surface charge reversible polymer composite[56] that respond to dual pH (cancer extra cellular pH of 6.5 and endosomal pH of 5). The composite flips its charge from negative to positive in the extra cellular matrix which facilitates the passive internalization of the composite through negatively charged lipid bilayer to the endosome.

In this chapter, we present gold nanorods- mesoporous silica hybrid material capable of flipping the charge from negative to positive at the extracellular pH to facilitate the passive internalization. We have also demonstrated the enhanced release of doxorubicin from the system at endosomal pH (5.0) in-vitro. Figure-2 schematically represents the concept of the work discussed in this chapter.

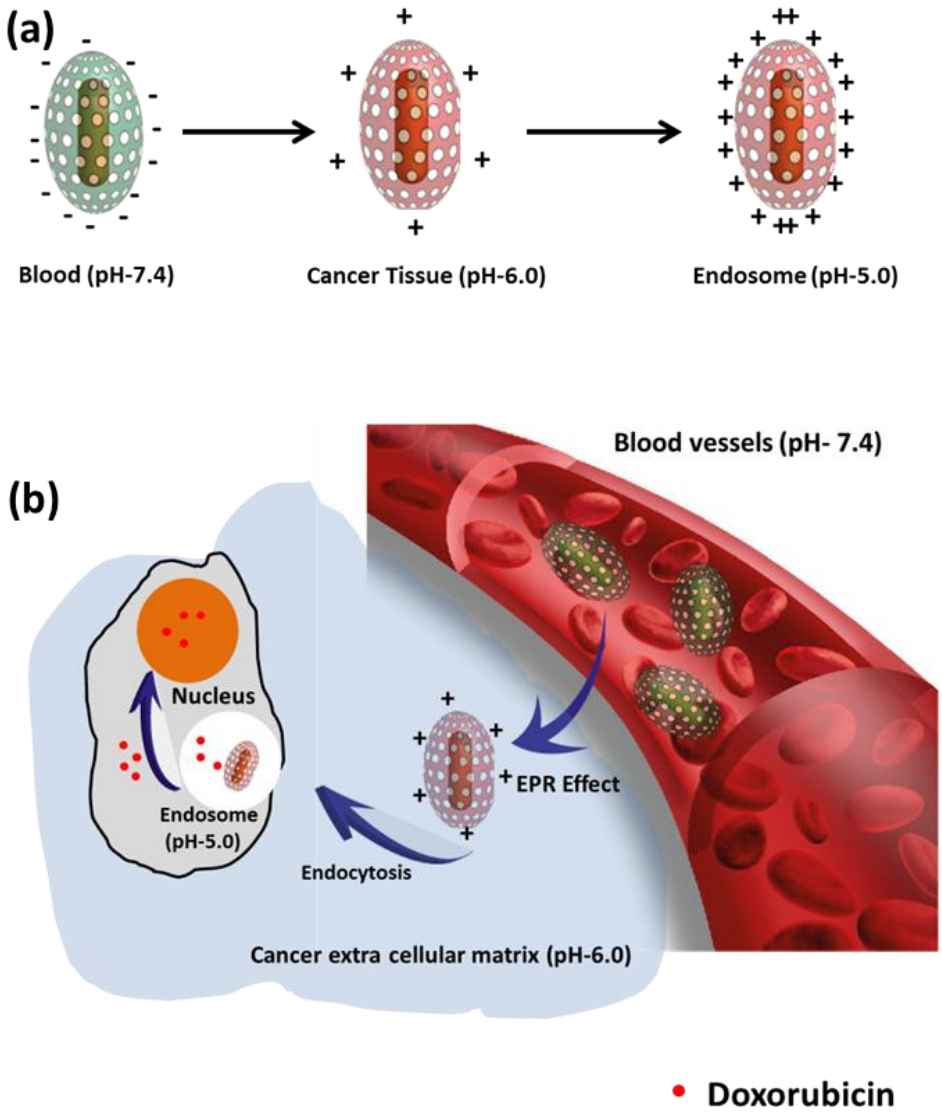

Figure-2: (a) Surface charge variation of $Au@SiO_2$ with respect to the pH. $Au@SiO_2$ is negatively charged at blood pH (7.4), becomes less positive (+10 mV) at cancerous tissue pH (6.0) and more positive (+30 mV) at endosomal pH (5.0). (b) Negatively charged $Au@SiO_2$ enters the cancerous extracellular matrix through EPR effect and changes its charge to positive, which enables entry to the cell through endocytosis to deliver doxorubicin at cytoplasm.

2.3 Experimental Methods:

2.3.1 Materials:

Gold(III) chloride trihydrate (Sigma Aldrich), silver nitrate (Sigma Aldrich), sodium borohydrate (SD Fine Chemicals), hexadecyltrimethylammonium bromide (CTAB) (Sigma Aldrich), ascorbic acid (SD Fine Chemicals), tetraethyl orthosilicate (Sigma Aldrich), (3-aminopropyl)triethoxysilane (Sigma Aldrich), sodium hydroxide (SD Fine Chemicals), doxorubicin (Cayman chemicals) and ninhydrin (Spectrochem) were used in this study as received.

2.3.2 Synthesis of Gold nanorods:

Gold nanorods were synthesized through seed mediated synthesis procedure as previously reported[41] with minor modifications.

Seed synthesis: Seed solution was prepared by mixing 1 mL of 0.5 mM $HAuCl_4$ solution and 1 mL of 0.2 M CTAB solution. The mixture was stirred for 2 minutes followed by the dropwise addition of 0.12 mL freshly prepared $NaBH_4$ (0.01 M) solution under stirring. The colour of the solution turned to brown indicating the formation of the gold seeds.

Growth solution: Growth solution was made by mixing 100 mL of 0.2 M CTAB solution, 5.6 mL of 4 mM $AgNO_3$ solution, 6.5 mL of 23 mM $HAuCl_4$ solution and 95 mL of deionized water. The mixture was vigorously stirred at 30 ^{0}C for 10 minutes. 2.5 mL of 0.08 M ascorbic acid was added dropwise to the growth solution with stirring. The colour of the solution changes from dark-orange to colourless. To this 1.8 mL of seed solution was added. The mixture was stirred vigorously for 1 minute and kept at 30 ^{0}C. The colour of the solution changes to dark-red within 20 minutes indicating the formation of gold nanorods.

2.3.3 Mesoporous silica coating over gold nanorods ($Au@SiO_2$):

75 mL of as-synthesized gold nanorods solution was centrifuged at 13,000 rpm for 25 minutes to remove excess CTAB. The precipitate of gold nanorods was dispersed in 50 mL deionized water with subsequent addition of 500 µL of 0.1 M NaOH solution. Three injections, each containing 150 µL of 20 % (v/v) tetraethylorthosilicate (TEOS) in methanol were added at an interval of 30 minutes. The mixture was allowed to react for 24 h. To remove the CTAB template, the red precipitate of mesoporous silica coated gold nanorods was dispersed in 20 mL ethanol containing 0.2 mL hydrochloric acid (0.12 M) and refluxed at 85 ^{0}C for 1 h. The precipitate was then centrifuged and washed with hot methanol several times. The template removed silica coated gold nanorods were then dried in vacuum for 3 h.

2.3.4 Aminopropyl functionalization of $Au@SiO_2$:

10 mg of the $Au@SiO_2$ was dispersed in dry acetonitrile by sonication. 30 µL APTES ((3-aminopropyl) triethoxysilane) was added to the dispersion. It was refluxed at 85 ^{0}C for 24 h to yield aminopropyl functionalized gold nanorods ($Au@SiO_2$-NH_2). The precipitate was then centrifuged and washed once with acetonitrile and thrice with hot methanol (40 ^{o}C), before drying it in vacuum for 3 h.

2.3.5 Estimation of primary amine groups in $Au@SiO_2$-NH_2:

Ninhydrin test was conducted to estimate the primary amine groups present in $Au@SiO_2$-NH_2. [55] Standard solutions of n-propylamine of various concentrations (0.2 – 1 mM) were made in absolute ethanol to serve as reference for calibration. 2.6 mg of amino-propyl functionalized $Au@SiO_2$ was dried in vacuum for 3 h prior to use and dispersed in 2 mL absolute ethanol by sonication for 30 minutes. 500 µL of freshly prepared (0.3 % w/v) ninhydrin solution was added to the dispersion and further sonicated for 15 minutes more. The sample-ninhydrin solution was kept at 65 ^{0}C for 30 minutes. The samples were cooled

down to room temperature and centrifuged. The supernatant was collected and analysed using UV-vis spectroscopy.

2.3.6 Loading of doxorubicin into Au@SiO_2-NH_2 and its release:

Doxorubicin stock solution of approximate concentration 0.2 mg/mL was prepared in 0.1 M PBS buffer of pH 7.4. Accurately weighed Au@SiO_2-NH_2 (1 mg) was dispersed in 1 mL doxorubicin stock solution. The dispersion was stirred for 24 h in dark. After loading, Au@SiO_2-NH_2 was washed twice with PBS buffer (pH- 7.4). All washings were collected and the amount of doxorubicin loaded was precisely calculated from UV-Vis absorption at 485 nm.

All release studies were performed at room temperature. 1 mg of Au@SiO_2-NH_2 was dispersed in 1 mL of 0.1 M PBS buffer. At predetermined time intervals, 500 µL aliquots of supernatant were taken to monitor the release of doxorubicin using UV-vis spectroscopy.

The entrapment efficiency (EE) was calculated as follows:

$$\mathrm{EE} = \frac{amount\ of\ drug\ loaded}{amount\ of\ drug\ in\ soaking\ solution\ before\ loading} \times 100$$

2.3.7 Characterization:

TEM images were acquired using TECNAI 200 kV Transmission electron microscope. FESEM images were acquired by Nova - Nano SEM – 600 (FEI, Netherlands). Powder XRD was obtained using Brucker-D8 diffractometer with Cu Kα radiation (λ=1.54 Å, Step size: 0.02, Current: 30 mA and Voltage: 40 kV). N_2 adsorption-desorption studies was carried out on Autosorb-1C (Quantachrome corp) at 77 K. Samples were outgassed at 85 ^{0}C for 12 h prior to adsorption measurements. The specific surface area and pore size distribution were calculated using the Quantachrome software (ASiQwin). UV-vis spectra were recorded

on a Perkin Elmer Lambda 900 UV-Vis-NIR spectrometer. FT-IR spectra were recorded on a Bruker IFS 66v/S spectrometer. Zeta potential measurements were carried out using a NanoZS (Malvern UK) instrument.

2.4 Results and Discussion:

Gold nanorods (AuNRs) were synthesised following typical seed mediated procedure. The TEM image (Figure-3a) shows gold nanorods of average length of 31 ± 2 nm and width 10 ± 1 nm. Figure-3b shows the electronic absorption spectrum of gold nanorods consisting of two distinct peaks. The peak at 515 nm corresponds to transverse surface plasmon resonance (TSPR) and the peak at 795 nm corresponds to longitudinal surface plasmon resonance (LSPR). LSPR is having higher molar absorption coefficient in comparison to the TSPR[57]. LSPR peak position is highly dependent on the aspect ratio of the gold nanorods. The average aspect ratio of gold nanorods is found to be 3.2 and it is matches with the LSPR peak position (795 nm) as previously reported.[57]

Figure-3c shows the zeta potential distribution of as-synthesised gold nanorods. The zeta potential of gold nanorods shows +25 mV mainly due to the presence of positively charged CTAB (cetyltrimethylammonium bromide) double layer over surface of the gold nanorods.[41]

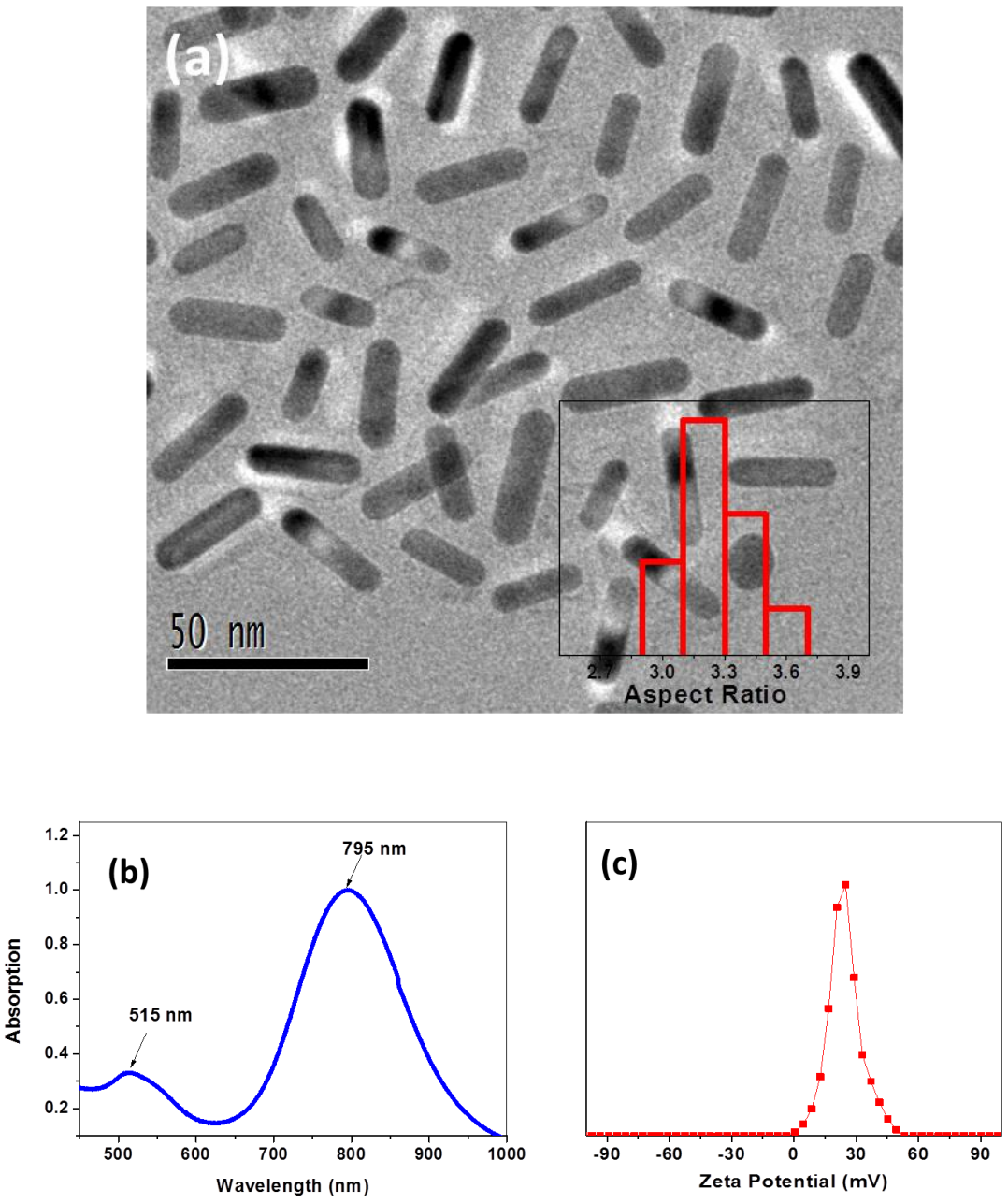

Figure-3: (a) TEM image of the as-synthesized gold nanorods. (b) Typical UV-Vis-NIR absorption spectrum of the gold nanorods. (c) Zeta potential distribution curve of the gold nanorods.

Mesoporous silica coating on the gold nanorods has been carried out in a single step using Stober method.[58] CTAB double layer adsorbed over the gold nanorod acts as template for the growth of the mesoporous silica on its surface. TEM image of the mesoporous silica coated gold nanorods (Figure-4a) clearly shows that the thickness of the silica coating is

around 20 nm and is porous in nature. Figure-4b and 4c show the FESEM images of the $Au@SiO_2$.

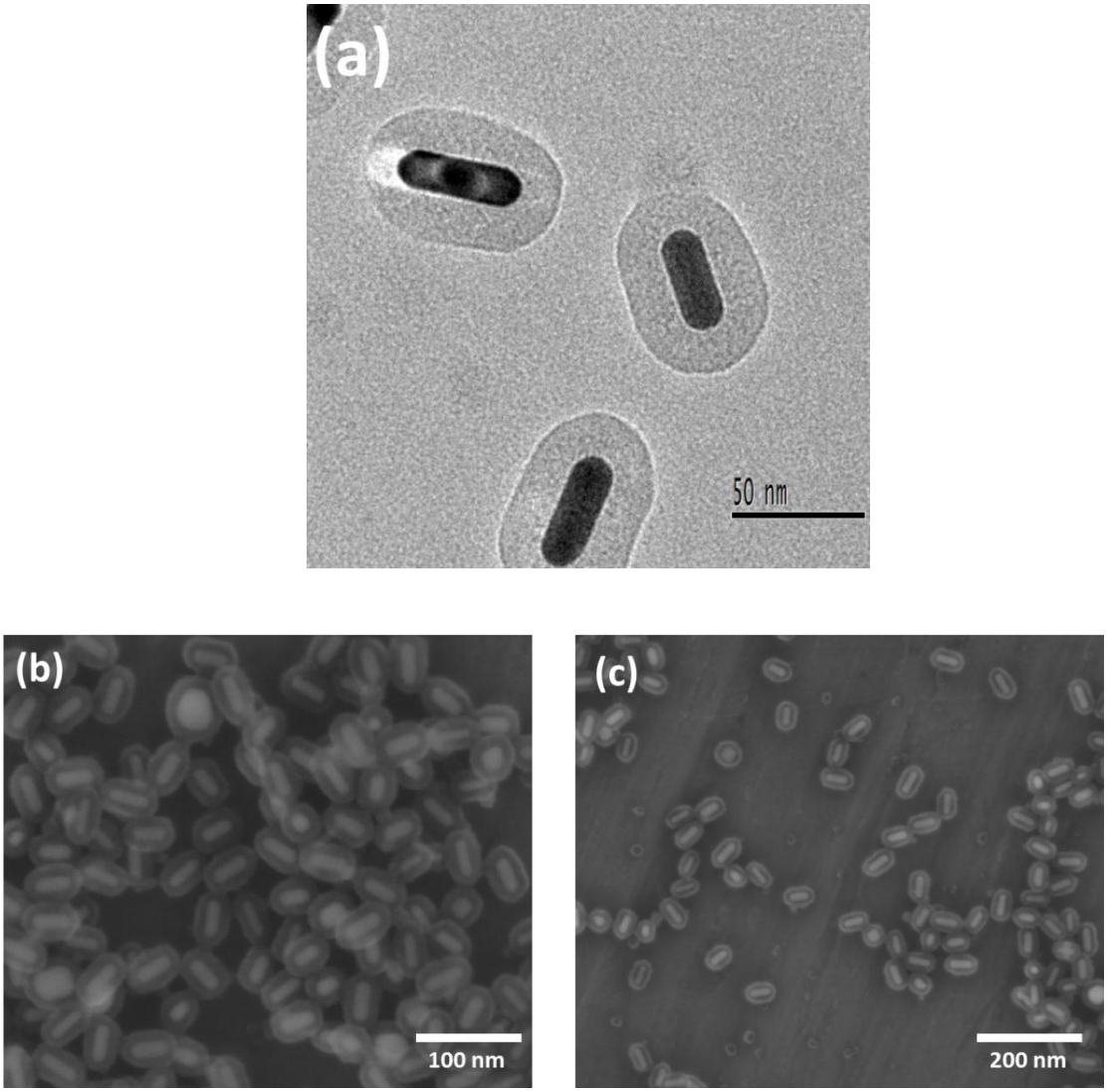

Figure-4: (a) TEM image of the mesoporous silica coated gold nanorods. (b) and (c) FESEM images of mesoporous silica coated gold nanorods at different magnifications.

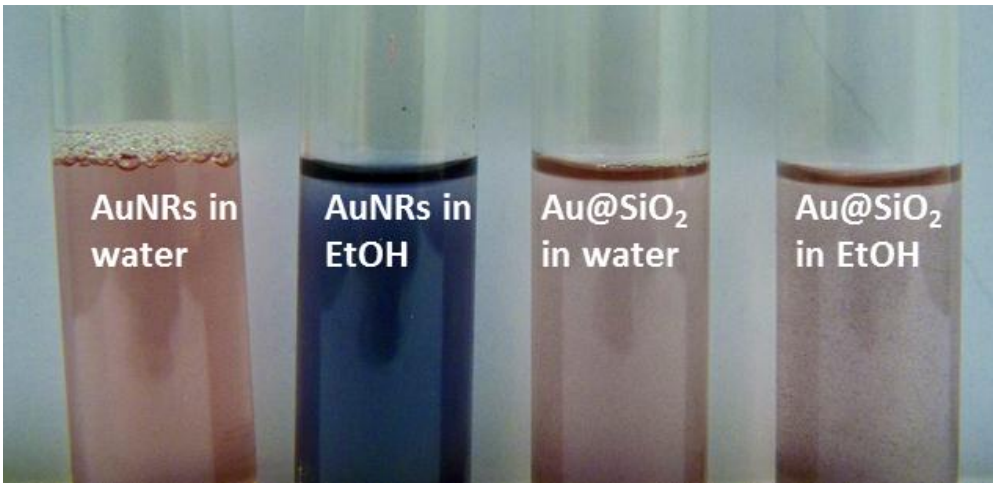

Figure-5: Photographs showing the stability of gold nanorods and silica coated gold nanorods in water and ethanol.

Mesoporous silica coating provides good stability to the gold nanorods. Figure-5 shows the stability of as-synthesized gold nanorods and $Au@SiO_2$ in water and ethanol. The positively charged CTAB double layer provides stability to the gold nanorods and prevents their aggregation in water. But, owing to the high solubility of CTAB in ethanol, gold nanorods readily aggregate in ethanol and lead to colour change due to shift in the plasmonic absorption as shown in Figure-5. Silica coating stabilizes the gold nanorods by preventing their aggregation through repulsive interaction of ionized silanol groups in the silica. This preserves the colour of the gold nanorods in ethanol.

The UV-vis absorption spectrum of silica coated gold nanorods (Figure- 6a) shows a 20 nm red-shift in the longitudinal plasmon absorption (815 nm) compared to the uncoated gold nanorods (795 nm). This is understandable considering the fact that the refractive index of silica shell (1.45) is larger than that of water (1.33). The transverse plasmon band remained same at 520 nm for both coated and uncoated gold nanorods as it is less affected by the small change in the metal-dielectric interface due to silica coating.[59] Figure-6b shows zeta potential of gold nanorods before and after silica coating. The uncoated gold nanorods dispersed in

water show a positive zeta potential (+30 mV) due to the bilayer coverage of CTAB whereas, silica coated gold nanorods show negative zeta potential (-24 mV) due to negatively charged silica surface.

FTIR spectrum of $Au@SiO_2$ (Figure-7a) shows all the significant vibrations relevant to silica. Vibrations at 486 cm^{-1} and 1100 cm^{-1} corresponds to Si-O-Si bending and stretching respectively, whereas 1618 cm^{-1} and 3395 cm^{-1} frequencies corresponding to bending and stretching vibrations of the absorbed water. Figure- 7b represents powder XRD pattern of the mesoporous silica coated gold nanorods which match clearly with the FCC lattice of gold.

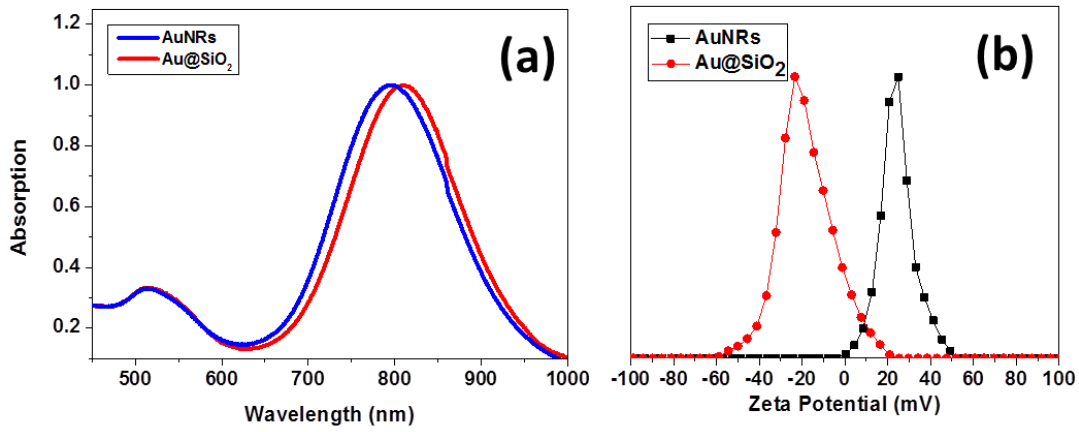

Figure-6: (a) UV-Vis-NIR absorption spectra before (AuNRs) and after silica coating ($Au@SiO_2$) on gold nanorods (b) Zeta potential distribution before and after silica coating on gold nanorods.

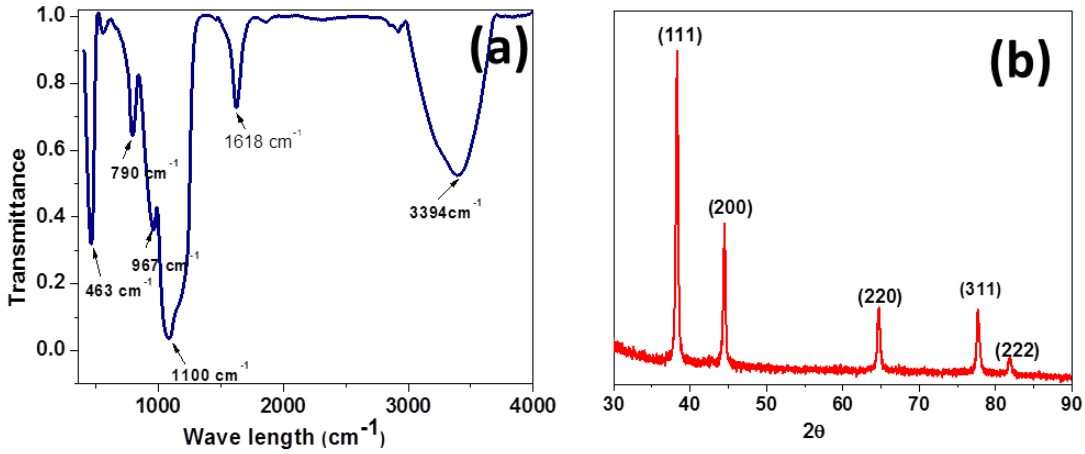

Figure-7: (a) FTIR spectrum of the silica coated gold nanorods. (b) PXRD pattern of the silica coated gold nanorods.

Mesoporous nature of the silica layer over gold nanorods is confirmed by the N_2 adsorption-desorption isotherm. Figure-8a shows the N_2 isotherm of $Au@SiO_2$ which is of type-IV according to IUPAC classification. A steep uptake of nitrogen at low P/P_0 is associated with micropore filling. The specific surface area calculated from BET (Brunauer–Emmett–Teller) equation is found to be 400 m^2/g and pore volume calculated at $P/P_0 = 0.98$ is 0.354 cc/g. Average pore size distribution calculated by using BJH (Barrett-Joyner-Halenda) method is about 3.2 nm (Figure-8b).

Aminopropyl functionalization of $Au@SiO_2$ particles was carried out by condensing 3-aminopropyltriethoxysilane (APTES) on to the silica surface of $Au@SiO_2$. Figure-9 shows FTIR spectra of $Au@SiO_2$ before and after aminopropyl functionalization. Asymmetric bending vibration of $-NH_2$ at 1500 cm^{-1} confirms the incorporation of amino-propyl to silica surface.

The amount of the primary amine groups in $Au@SiO_2$-NH_2 was estimated using Ninhydrin test, typically used for the quantification of the amine groups in the amino acids.[59]

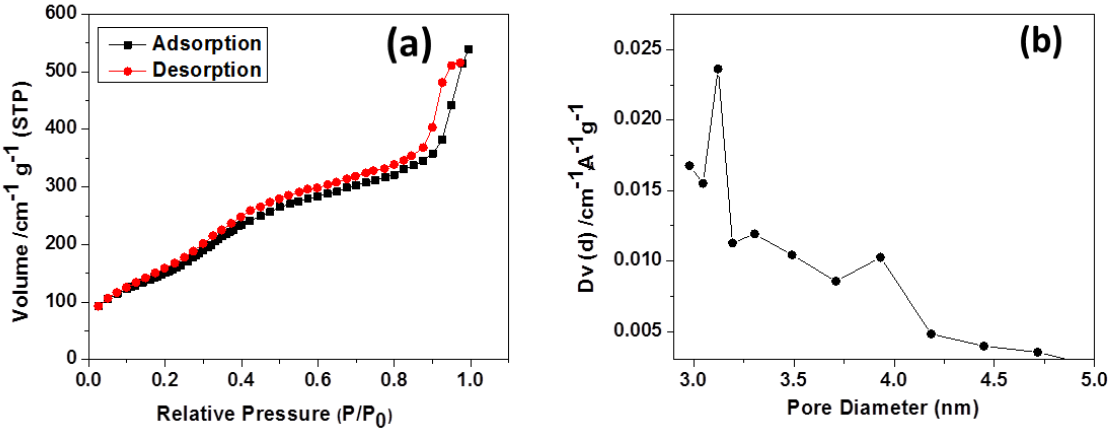

Figure-8: (a) Nitrogen adsorption-desorption isotherm and (b) Barrett-Joyner-Halenda pore size distribution curve of mesoporous silica coated gold nanorods.

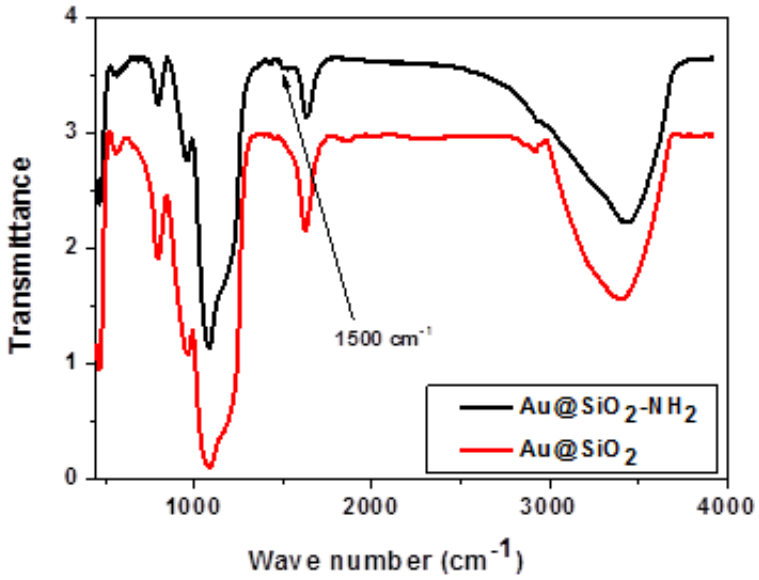

Figure-9: FTIR spectra of the mesoporous silica coated gold nanorods before and after APTES functionalization.

A calibration plot of ninhydrin complex has been made using n-propylamine as standard (Figure-10a&b). Using the calibration plot the amine groups present in $Au@SiO_2$-NH_2 were quantified and found to be 0.6 mmol g^{-1}.

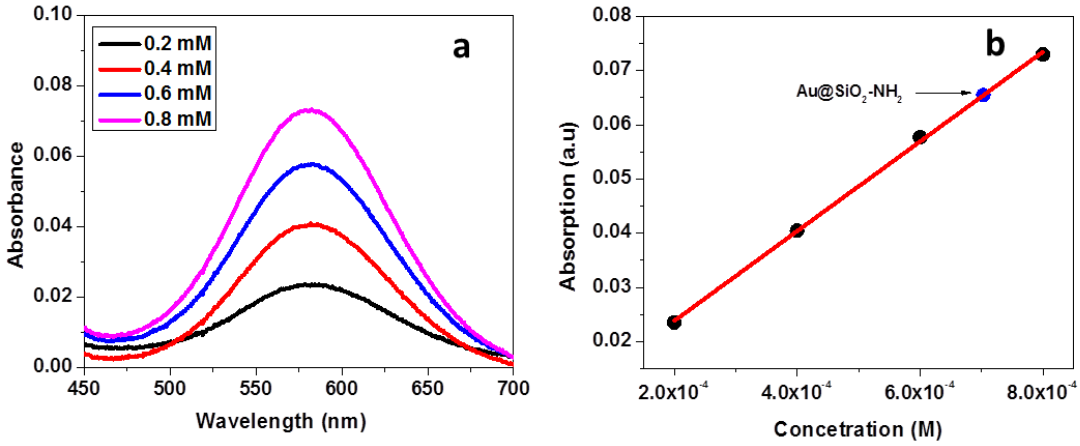

Figure-10: (a) UV-visible spectra of the ninhydrin complex in the calibration solutions. (b) Calibration plot showing increase in absorbance monitored at 580 nm with increase in n-propylamine used in the standard solution.

Zeta potential measurements (Figure-11) show that Au@`SiO_2-NH_2 exhibit charge reversal with respect to pH. At pH 7.4, it shows a negative potential of -7.8 mV which change to positive value (+30 mV) at pH 5. On the other hand, zeta potential shows no charge reversal for Au@SiO_2. It shows a variation only in the negative regime from -21 mV at pH 7.4 to -5 mV at pH 5. It is understandable by recalling that the negative charge comes from the ionization of the silanol groups.[60] At pH 7.4, more number of the silanol groups would be ionized making it more negatively charged. At pH 5, the silanol ionization is lesser thus lowering the net negative charge. At pH 7.4, the surface of Au@SiO_2-NH_2 is less negative (-7.8 mV) than that of Au@SiO_2 (-20 mV). As the pH is lowered to 6 the surface becomes positive (+4.4 mV) due to increased protonation of the amine groups and diminished silanol ionization.

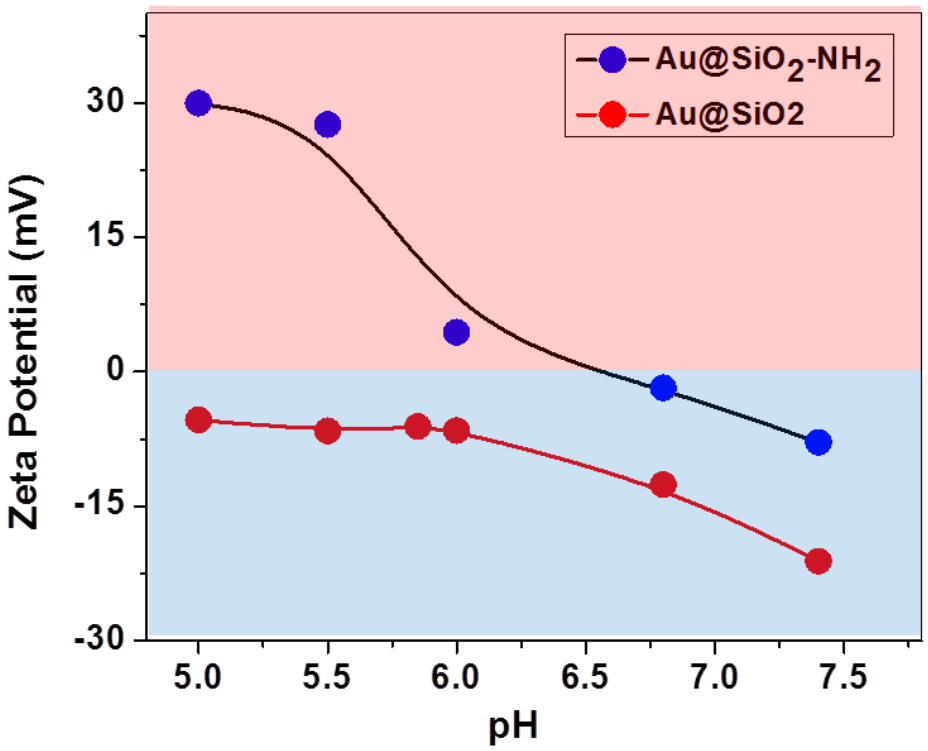

Figure-11: Zeta potential variation with respect to pH for $Au@SiO_2$ and $Au@SiO_2$-NH_2.

The existence of the weak acidic environment (pH 6) at the cancerous extracellular matrix would help $Au@SiO_2$-NH_2 to acquire positive charge which is essential for its cellular entry through electrostatic interaction with negatively charged cell wall. Inside the cell, the endosomal pH is even more acidic (pH-5) which make $Au@SiO_2$-NH_2 particle more positive. Acquisition of strong positive charge by $Au@SiO_2$-NH_2 particles is expected to facilitate the release of positively charged anti-cancer drugs such as doxorubicin.

Doxorubicin which is a well-known anticancer drug is loaded into the pores of $Au@SiO_2$-NH_2. Structure of the doxorubicin is given in Figure-12. Loading of doxorubicin was done at pH 7.4. At this pH $Au@SiO_2$-NH_2 is negatively charged and doxorubicin is

positively charged[61] as its pK_a is about 7.6 leading to high entrapment efficiency nearly 64.5% (w/w).

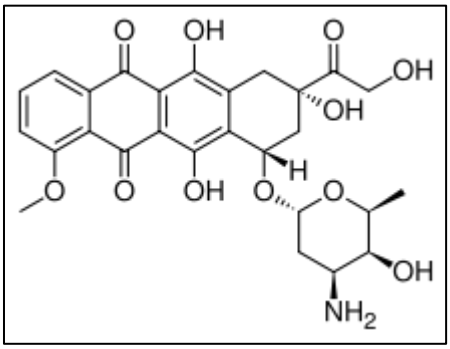

Figure-12: Chemical Structure of the drug Doxorubicin (trade name Adriamycin).

The release of doxorubicin from Au@SiO_2-NH_2 at different pH is given in Figure-13a. A high release of doxorubicin (55 % in 8 h) is shown by Au@SiO_2-NH_2 at pH-5 (endosomal pH) due to the repulsive interaction between the positively charged drug and positive Au@SiO_2-NH_2. In normal extracellular pH (i.e. 7.4) a low release was observed due to the attractive interaction between the drug and negatively charged Au@SiO_2-NH_2.

As a control, doxorubicin release from Au@SiO_2 was studied and the result shown in Figure-13b. Doxorubicin was loaded to Au@SiO_2 at pH 7.4 with an entrapment efficiency of 63%. Release kinetics for Au@SiO_2 shows a maximum release of doxorubicin is at pH 5 which is about 20 % in 12 h. It is interesting to note that this release is almost same as that of Au@SiO_2-NH_2 at 7.4 which can be explained by the fact that both Au@SiO_2 and Au@SiO_2-NH_2 having same magnitude of negative charge at pH 7 and 5 respectively. Table-1 summarizes the surface charges and releases at different pH for Au@SiO_2- NH_2 and Au@SiO_2.

Amount of doxorubicin released in release studies was calculated using a calibration curve made from known concentrations of doxorubicin. Figure-14a-b shows calibration curve for doxorubicin.

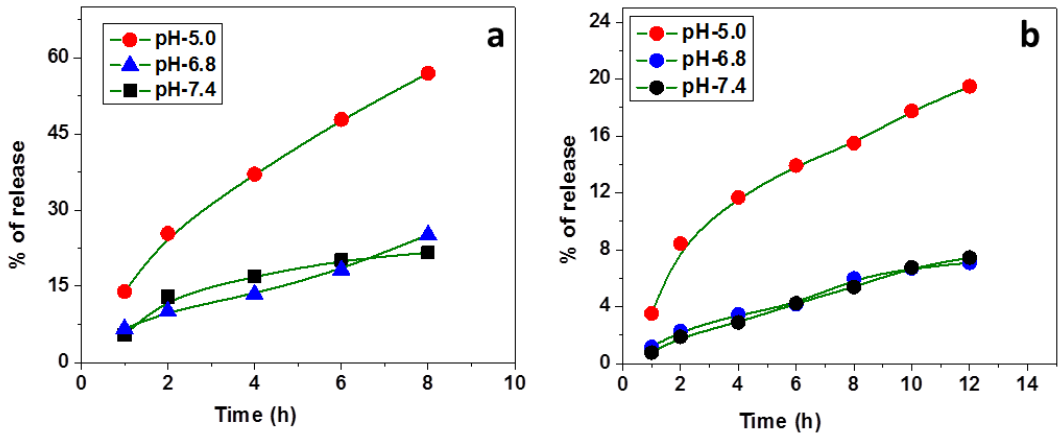

Figure-13: (a) Doxorubicin release from Au@SiO_2- NH_2 at different pH. (b) Doxorubicin release from Au@SiO_2 at different pH.

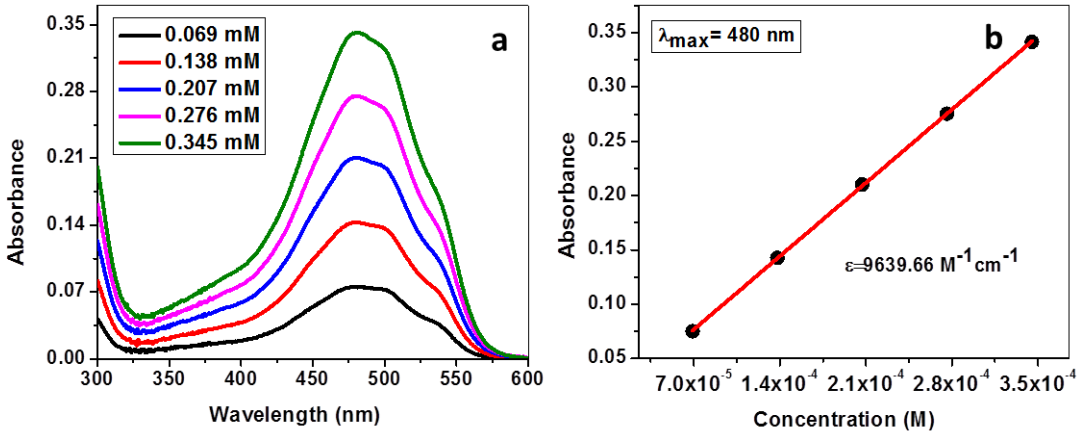

Figure-14: (a) UV-visible spectra of the doxorubicin in calibration solutions. (b) Linear calibration plot.

	Surface Charge		Release after 8h	
	pH-7.4	pH-5	pH-7.4	pH-5
$Au@SiO_2$- NH_2	-8.0 mV	+30.0 mV	21.6%	57.0%
$Au@SiO_2$	-21.1 mV	-5.3 mV	5.0%	16.0%

Table-1: Summary of the surface charge variation and release of doxorubicin for both $Au@SiO_2$- NH_2 and $Au@SiO_2$ with respect to pH.

2.5 Conclusion:

We have synthesised mesoporous silica coated gold nanorods and demonstrated the use of this system for anti-cancer drug delivery. Mesoporous coating has shown promising surface area and high specific volume which was- utilized for the loading of doxorubicin - a well-known anti-cancer drug. The charge reversal of the designed system from negative to positive as pH varies from 7.4 to 5 is used for the effective release of the cargo at endosomal pH. The surface charge reversal from negative to less positive can also be used for the passive cell entry facilitated through the electrostatic interactions between negatively charged lipid layer and positively charged gold –silica hybrid.

2.6 References:

1 Siegel, R., Naishadham, D. & Jemal, A. Cancer statistics, 2012. *CA-Cancer J. Clin.* **62**, 10-29, (2012).

2 Siegel, R., Naishadham, D. & Jemal, A. Cancer statistics, 2013. *CA-Cancer J. Clin.* **63**, 11-30, (2013).

3 Ries, L. A. G., Melbert, D., Krapcho, M., Stinchcomb, D. G., Howlader, N., Horner, M. J., Mariotto, A., Miller, B. A., Feuer, E. J., Altekruse, S. F., Lewis, D. R., Clegg, L., Eisner, M. P., Reichman, M. & Edwards, B. K. SEER cancer statistics review, 1975-2005. (U.S. National Institutes of Health, National Cancer Institute, Bethesda, MD, 2008).

4 Mura, S., Nicolas, J. & Couvreur, P. Stimuli-responsive nanocarriers for drug delivery. *Nat Mater* **12**, 991-1003, (2013).

5 Scheinberg, D. A., Villa, C. H., Escorcia, F. E. & McDevitt, M. R. Conscripts of the infinite armada: systemic cancer therapy using nanomaterials. *Nat Rev Clin Oncol* **7**, 266-276, (2010).

6 Nel, A. E., Madler, L., Velegol, D., Xia, T., Hoek, E. M. V., Somasundaran, P., Klaessig, F., Castranova, V. & Thompson, M. Understanding biophysicochemical interactions at the nano-bio interface. *Nat Mater* **8**, 543-557, (2009).

7 Farokhzad, O. C. & Langer, R. Impact of Nanotechnology on Drug Delivery. *ACS Nano* **3**, 16-20, (2009).

8 Danhier, F., Feron, O. & Préat, V. To exploit the tumor microenvironment: Passive and active tumor targeting of nanocarriers for anti-cancer drug delivery. *J. Controlled Release* **148**, 135-146, (2010).

9 Adair, J. H., Parette, M. P., Altınoğlu, E. İ. & Kester, M. Nanoparticulate Alternatives for Drug Delivery. *ACS Nano* **4**, 4967-4970, (2010).

10 Byrne, J. D., Betancourt, T. & Brannon-Peppas, L. Active targeting schemes for nanoparticle systems in cancer therapeutics. *Adv. Drug Deliv. Rev.* **60**, 1615-1626, (2008).

11 Singh, R. & Lillard Jr, J. W. Nanoparticle-based targeted drug delivery. *Exp. Mol. Pathol* **86**, 215-223, (2009).

12 Cho, K., Wang, X., Nie, S., Chen, Z. & Shin, D. M. Therapeutic Nanoparticles for Drug Delivery in Cancer. *Clinical Cancer Research* **14**, 1310-1316, (2008).

13 Torchilin, V. Tumor delivery of macromolecular drugs based on the EPR effect. *Adv. Drug Deliv. Rev.* **63**, 131-135, (2011).

14 Maeda, H., Wu, J., Sawa, T., Matsumura, Y. & Hori, K. Tumor vascular permeability and the EPR effect in macromolecular therapeutics: a review. *J. Controlled Release* **65**, 271-284, (2000).

15 Maeda, H., Sawa, T. & Konno, T. Mechanism of tumor-targeted delivery of macromolecular drugs, including the EPR effect in solid tumor and clinical overview of the prototype polymeric drug SMANCS. *J. Controlled Release* **74**, 47-61, (2001).

16 Cheng, C. J. & Saltzman, W. M. Nanomedicine: Downsizing tumour therapeutics. *Nat Nano* **7**, 346-347, (2012).

17 Alarcon, C. d. l. H., Pennadam, S. & Alexander, C. Stimuli responsive polymers for biomedical applications. *Chem. Soc. Rev.* **34**, 276-285, (2005).

18 Ganta, S., Devalapally, H., Shahiwala, A. & Amiji, M. A review of stimuli-responsive nanocarriers for drug and gene delivery. *J. Controlled Release* **126**, 187-204, (2008).

19 Schmaljohann, D. Thermo- and pH-responsive polymers in drug delivery. *Adv. Drug Deliv. Rev.* **58**, 1655-1670, (2006).

20 Wu, X. L., Kim, J. H., Koo, H., Bae, S. M., Shin, H., Kim, M. S., Lee, B.-H., Park, R.-W., Kim, I.-S., Choi, K., Kwon, I. C., Kim, K. & Lee, D. S. Tumor-Targeting

Peptide Conjugated pH-Responsive Micelles as a Potential Drug Carrier for Cancer Therapy. *Bioconjugate Chem.* **21**, 208-213, (2010).

21 Su, J., Chen, F., Cryns, V. L. & Messersmith, P. B. Catechol Polymers for pH-Responsive, Targeted Drug Delivery to Cancer Cells. *J. Am. Chem. Soc.* **133**, 11850-11853, (2011).

22 Bae, Y., Fukushima, S., Harada, A. & Kataoka, K. Design of Environment-Sensitive Supramolecular Assemblies for Intracellular Drug Delivery: Polymeric Micelles that are Responsive to Intracellular pH Change. *Angew. Chem. Int. Ed.* **42**, 4640-4643, (2003).

23 Rapoport, N. Physical stimuli-responsive polymeric micelles for anti-cancer drug delivery. *Prog. Polym. Sci.* **32**, 962-990, (2007).

24 Tang, L.-Y., Wang, Y.-C., Li, Y., Du, J.-Z. & Wang, J. Shell-Detachable Micelles Based on Disulfide-Linked Block Copolymer As Potential Carrier for Intracellular Drug Delivery. *Bioconjugate Chem.* **20**, 1095-1099, (2009).

25 Patel, K., Angelos, S., Dichtel, W. R., Coskun, A., Yang, Y.-W., Zink, J. I. & Stoddart, J. F. Enzyme-Responsive Snap-Top Covered Silica Nanocontainers. *J. Am. Chem. Soc.* **130**, 2382-2383, (2008).

26 Alvarez-Lorenzo, C., Bromberg, L. & Concheiro, A. Light-sensitive Intelligent Drug Delivery Systems†. *Photochem. Photobiol.* **85**, 848-860, (2009).

27 Giri, S., Trewyn, B. G., Stellmaker, M. P. & Lin, V. S. Y. Stimuli-Responsive Controlled-Release Delivery System Based on Mesoporous Silica Nanorods Capped with Magnetic Nanoparticles. *Angew. Chem. Int. Ed.* **44**, 5038-5044, (2005).

28 Murdan, S. Electro-responsive drug delivery from hydrogels. *J. Controlled Release* **92**, 1-17, (2003).

29 Katz, J. S. & Burdick, J. A. Light-Responsive Biomaterials: Development and Applications. *Macromolecular Bioscience* **10**, 339-348, (2010).

30 Schwarz, A., Stander, S., Berneburg, M., Bohm, M., Kulms, D., van Steeg, H., Grosse-Heitmeyer, K., Krutmann, J. & Schwarz, T. Interleukin-12 suppresses ultraviolet radiation-induced apoptosis by inducing DNA repair. *Nat Cell Biol* **4**, 26-31, (2002).

31 Kang, H., Trondoli, A. C., Zhu, G., Chen, Y., Chang, Y.-J., Liu, H., Huang, Y.-F., Zhang, X. & Tan, W. Near-Infrared Light-Responsive Core–Shell Nanogels for Targeted Drug Delivery. *ACS Nano* **5**, 5094-5099, (2011).

32 Liu, J., Bu, W., Pan, L. & Shi, J. NIR-Triggered Anticancer Drug Delivery by Upconverting Nanoparticles with Integrated Azobenzene-Modified Mesoporous Silica. *Angew. Chem. Int. Ed.* **52**, 4375-4379, (2013).

33 Hahn, G. M. Metabolic Aspects of the Role of Hyperthermia in Mammalian Cell Inactivation and Their Possible Relevance to Cancer Treatment. *Cancer Research* **34**, 3117-3123, (1974).

34 Li, N., Zhao, P. & Astruc, D. Anisotropic Gold Nanoparticles: Synthesis, Properties, Applications, and Toxicity. *Angew. Chem. Int. Ed.* **53**, 1756-1789, (2014).

35 Huang, X., Neretina, S. & El-Sayed, M. A. Gold Nanorods: From Synthesis and Properties to Biological and Biomedical Applications. *Adv. Mater.* **21**, 4880-4910, (2009).

36 Kennedy, L. C., Bickford, L. R., Lewinski, N. A., Coughlin, A. J., Hu, Y., Day, E. S., West, J. L. & Drezek, R. A. A New Era for Cancer Treatment: Gold-Nanoparticle-Mediated Thermal Therapies. *Small* **7**, 169-183, (2011).

37 Hu, X. & Gao, X. Multilayer coating of gold nanorods for combined stability and biocompatibility. *Phys. Chem. Chem. Phys.* **13**, 10028-10035, (2011).

38 Niidome, T., Yamagata, M., Okamoto, Y., Akiyama, Y., Takahashi, H., Kawano, T., Katayama, Y. & Niidome, Y. PEG-modified gold nanorods with a stealth character for in vivo applications. *J. Controlled Release* **114**, 343-347, (2006).

39 Wilson, C. G., Sisco, P. N., Gadala-Maria, F. A., Murphy, C. J. & Goldsmith, E. C. Polyelectrolyte-coated gold nanorods and their interactions with type I collagen. *Biomaterials* **30**, 5639-5648, (2009).

40 Chen, Y.-S., Frey, W., Kim, S., Kruizinga, P., Homan, K. & Emelianov, S. Silica-Coated Gold Nanorods as Photoacoustic Signal Nanoamplifiers. *Nano Lett.* **11**, 348-354, (2011).

41 Gorelikov, I. & Matsuura, N. Single-Step Coating of Mesoporous Silica on Cetyltrimethyl Ammonium Bromide-Capped Nanoparticles. *Nano Lett.* **8**, 369-373, (2007).

42 Slowing, I. I., Vivero-Escoto, J. L., Wu, C.-W. & Lin, V. S. Y. Mesoporous silica nanoparticles as controlled release drug delivery and gene transfection carriers. *Adv. Drug Deliv. Rev.* **60**, 1278-1288, (2008).

43 Argyo, C., Weiss, V., Bräuchle, C. & Bein, T. Multifunctional Mesoporous Silica Nanoparticles as a Universal Platform for Drug Delivery. *Chem. Mater.* **26**, 435-451, (2013).

44 Lu, J., Liong, M., Li, Z., Zink, J. I. & Tamanoi, F. Biocompatibility, Biodistribution, and Drug-Delivery Efficiency of Mesoporous Silica Nanoparticles for Cancer Therapy in Animals. *Small* **6**, 1794-1805, (2010).

45 Slowing, I., Trewyn, B. G. & Lin, V. S. Y. Effect of Surface Functionalization of MCM-41-Type Mesoporous Silica Nanoparticles on the Endocytosis by Human Cancer Cells. *J. Am. Chem. Soc.* **128**, 14792-14793, (2006).

46 Zhang, Z., Wang, L., Wang, J., Jiang, X., Li, X., Hu, Z., Ji, Y., Wu, X. & Chen, C. Mesoporous Silica-Coated Gold Nanorods as a Light-Mediated Multifunctional Theranostic Platform for Cancer Treatment. *Adv. Mater.* **24**, 1418-1423, (2012).

47 Yang, X., Liu, X., Liu, Z., Pu, F., Ren, J. & Qu, X. Near-Infrared Light-Triggered, Targeted Drug Delivery to Cancer Cells by Aptamer Gated Nanovehicles. *Adv. Mater.* **24**, 2890-2895, (2012).

48 Marchant, G. E. Small is Beautiful: What Can Nanotechnology Do for Personalized Medicine? *Current Pharmacogenomics and Personalized Medicine* **7**, 231-237, (2009).

49 Jain, K. K. Role of nanobiotechnology in the development of personalized medicine. *Nanomedicine* **4**, 249-252, (2009).

50 Jain, K. K. in *Pharmaceutical Biotechnology* 553-580 (Wiley-VCH Verlag GmbH & Co. KGaA, 2012).

51 Pollok, S., Ginter, T., Günzel, K., Pieper, J., Henke, A., Stauber, R. H., Reichardt, W. & Krämer, O. H. Interferon alpha-armed nanoparticles trigger rapid and sustained STAT1-dependent anti-viral cellular responses. *Cellular Signalling* **25**, 989-998, (2013).

52 Vemula, P. K., Cruikshank, G. A., Karp, J. M. & John, G. Self-assembled prodrugs: An enzymatically triggered drug-delivery platform. *Biomaterials* **30**, 383-393, (2009).

53 Thévenin, D., An, M. & Engelman, D. M. pHLIP-Mediated Translocation of Membrane-Impermeable Molecules into Cells. *Chemistry & Biology* **16**, 754-762, (2009).

54 Goesmann, H. & Feldmann, C. Nanoparticulate Functional Materials. *Angew. Chem. Int. Ed.* **49**, 1362-1395, (2010).

55 Bassyouni, F., ElHalwany, N., Abdel Rehim, M. & Neyfeh, M. Advances and new technologies applied in controlled drug delivery system. *Res. Chem. Intermed.*, 1-36, (2013).

56 Du, J.-Z., Du, X.-J., Mao, C.-Q. & Wang, J. Tailor-Made Dual pH-Sensitive Polymer–Doxorubicin Nanoparticles for Efficient Anticancer Drug Delivery. *J. Am. Chem. Soc.* **133**, 17560-17563, (2011).

57 Orendorff, C. J. & Murphy, C. J. Quantitation of Metal Content in the Silver-Assisted Growth of Gold Nanorods. *J. Phys. Chem. B* **110**, 3990-3994, (2006).

58 Wong, Y. J., Zhu, L., Teo, W. S., Tan, Y. W., Yang, Y., Wang, C. & Chen, H. Revisiting the Stöber Method: Inhomogeneity in Silica Shells. *J. Am. Chem. Soc.* **133**, 11422-11425, (2011).

59 Wang, C. & Irudayaraj, J. Gold Nanorod Probes for the Detection of Multiple Pathogens. *Small* **4**, 2204-2208, (2008).

60 Meziani, M. J., Zajac, J., Jones, D. J., Rozière, J. & Partyka, S. Surface Characterization of Mesoporous Silicoaluminates of the MCM-41 Type: Evaluation of Polar Surface Sites Using Flow Calorimetry, Adsorption of a Cationic Surfactant as a Function of Pore Size and Aluminum Content. *Langmuir* **13**, 5409-5417, (1997).

61 Dalmark, M. Characteristics of doxorubicin transport in human red blood cells. *Scand J Clin Lab Invest* **41**, 633-639, (1981).

Chapter-3

Charge Transfer Assisted Strategy for Reversible End-to-End Assembly of Gold Nanorods

Summary:

This chapter deals with a new strategy adopted for the one dimensional self-assembly of the gold nanorods of type *AA or AB* in an end-to-end fashion. The strategy involves effective charge-transfer interaction between the donor acceptor molecules linked with plasmonic nanorods. We have synthesized donor and acceptor molecules for the assembly of gold nanorods. The binding kinetics and reversibility of charge-transfer complex were investigated for the donor-acceptor pair.

3.1 Introduction

Over the past few decades, organization of metal nanoparticles to one-, two-, or three dimensional superstructures has received a lot of interest.[1-3] The superstructured nanoparticles possess new fundamental information about the collective behavior of the individual nanoparticles which are either plasmonically or electronically coupled with each other.[4,5] Among various assembly structures, one dimensionally assembled metal nanoparticles gain importance mainly because of its resemblance with molecular polymers and its technological applications.[6,7] Stephen Link et al. first introduced the term plasmonic polymer to address one dimensional assembly of plasmonic nanoparticles.[8] They are unique due to the strong plasmonic interaction between the repeated nanoparticles. To date, plasmonic polymers found applications in sensing[9], nanocircuits[10], optical wave guiding[11], 'hot spot' generation[12] etc. The plasmonic polymer generated by end-to-end self-assembly of gold nanorods is unique and well-studied. The most important aspect of such plasmonic polymers is their longitudinal surface plasmon resonance (LSPR).[13] The LSPR of gold nanorods is highly sensitive to the surrounding medium[14] and highly susceptible for interparticles plasmon coupling.[15] Thus the optical properties of gold nanorods can be tuned by the extent of self-assembly, inter particles spacing and orientation between the gold nanorods.[16]

Various strategies are used for the end-to-end self-assembly of gold nanorods. Solvent induced aggregation of polystyrene moieties tethered to the ends of gold nanorods is one of the most popular methods.[13] Hydrophobic interaction of the polystyrene moieties in an appropriate solvent is utilized in this process. Though the assembly is reversible with respect to the solvent, considering the instability of gold nanorods in various organic solvents, a careful selection of solvent is required for the assembly- disassembly procedure.[17] Another popular strategy involves specific biomolecules interactions such as biotin – streptavidin[18], DNA base pairing[19] etc. pH dependent self-assembly of gold nanorods is also reported which typically involves electrostatic interactions.[20,21] All these approaches are significant in terms

of various applications. For instance, end-to-end assembly has been successfully employed for the detection of mercury[19], cysteine and glutathione[21] etc.

3.2 Scope of the present study

In this report, we have used a reversible, charge-transfer (CT) based strategy for the end-to-end assembly of gold nanorods. To our knowledge there are no reports on reversible, CT based self-assembly (through donor-acceptor interaction) of metal nanorods which has the resemblance to the controlled molecular polymerization.

We have used viologen-thiol **(1)** as the electron acceptor[22] which can be anchored to the ends of gold nanorods through strong Au-S covalent bond. 8-Hydroxy pyrene 1, 3, 6-trisulfonate (HPTS) **(3)**[23] based ligand was synthesized and used as an electron donor which can be attached to the ends of gold nanorods through metal-thiol covalent bond. One dimensional end-to-end assembly of gold nanorods could be initiated when the CT interaction between the donor and acceptor anchored on to the metal nanoparticle is established. These self-assembled structures can be reversibly disassembled and reassembled by reduction and oxidation of the viologen moiety respectively. On reduction viologen is converted to the radical cation structure resulting in lapse of CT interaction; subsequent oxidation of the species back to viologen reforms the assembly. The schematic representation of the concept presented in this chapter is given in Figure-1.

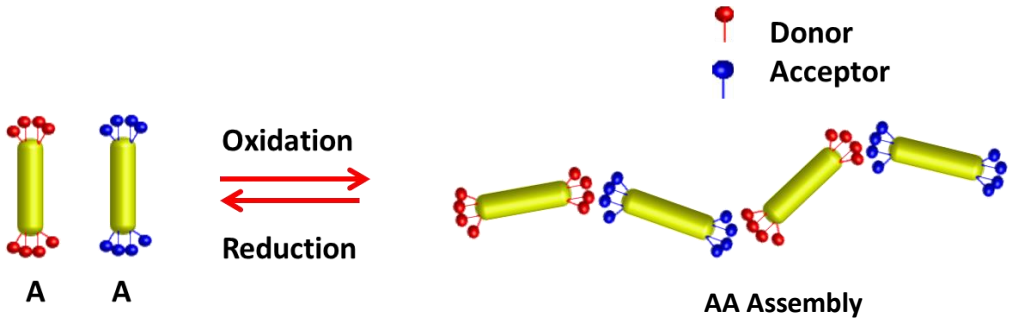

Figure-1: Schematic representation of the charge transfer assisted metal nanoparticles assembly strategy. The gold nanorods are assembled when charge transfer is established between the donor and acceptor molecules anchored to the ends of gold nanorod. The assembly is reversible with redox stimuli.

3.3 Experimental Methods

3.3.1 Materials:

Gold(III) chloride trihydrate (Sigma Aldrich), silver nitrate (Sigma Aldrich), sodium borohydrate (SD Fine Chemicals), hexadecyltrimethylammonium bromide (CTAB) (Sigma Aldrich), ascorbic acid (SD Fine Chemicals), 1-pyrenecarboxylic acid (Sigma Aldrich), sodium borohydrate (SD Fine Chemicals), 16-mercaptohexadecanoic acid (Sigma Aldrich), N,N'-dicyclohexylcarbodiimide (Sigma Aldrich), 4-dimethylaminopyridine (SD Fine Chemicals), trisodium 8-hydroxypyrene-1,3,6-trisulfonate (HPTS) (Alfa Aesar), N,N-diisopropylethylamine (Sigma Aldrich), 10-Bromo-1-decanol (TCl Chemicals) were used in this study as received.

3.3.2 Synthesis of Gold nanorods:

Gold nanorods were synthesized through seed mediated synthesis procedure as previously reported.[24]

Seed synthesis: Seed was prepared by mixing 1 mL of 0.5 mM $HAuCl_4$ solution and 1 mL of 0.2M CTAB solution. The mixture was stirred for 2 minutes and 0.12 mL of

freshly prepared $NaBH_4$ (0.01 M) was added dropwise for 1 minute under stirring. The colour of the solution turned to brown indicating the formation of the gold seeds.

Growth solution: Growth solution was made by mixing 50 mL of 0.2 M CTAB solution, 2.8 mL of 4 mM $AgNO_3$ solution, 3.2 mL of 23 mM $HAuCl_4$ solution and 45 mL deionized water. The mixture was vigorously stirred at 30 ^{0}C for 10 minutes. To this 1.2 mL of 0.08 M ascorbic acid was added dropwise under stirring. The colour of the solution changes from dark-orange to colourless. To this 1.8 mL seed solution was added. The mixture was stirred vigorously for 1 minute and kept at 30 ^{0}C. The colour of the solution changes to dark-red within 20 min indicating the formation of gold nanorods.

3.3.3 Synthesis of 1-methyl-4,4'-bipyridiniumundecanethiol (1):

Methyl viologen containing ligands (1-methyl-4,4'-bipyridiniumnonanethiol) was kindly donated by Dr. Subi Jacob George's group at New Chemistry Unit, JNCASR. The ligand was prepared by coupling 11-bromoundecanethiol and 1-methyl viologen. The scheme of the reaction is given below.

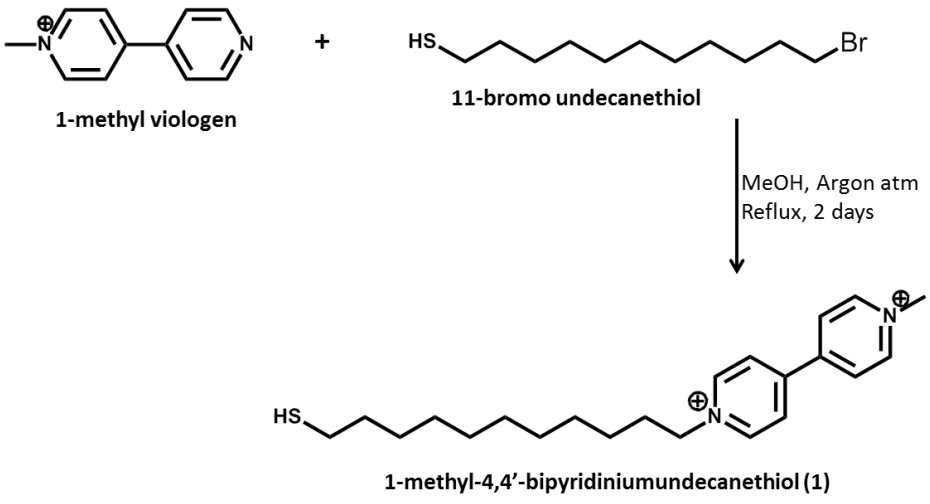

3.3.4 Synthesis of 8-(10-hydroxydecyl) oxy pyrene-1,3,6-trisulfonate (2):

10-Bromo-1-decanol (4.02 mmol) was added to a refluxing solution of trisodium 8-hydroxypyrene-1,3,6-trisulfonate (596.5 mg, 1.14 mmol) in MeOH containing N,N-

diisopropylethylamine (0.5 mL, 2.94 mmol), and the resulting mixture was refluxed with stirring for 6 days. The mixture was cooled down to room temperature and crude product was purified using column chromatography (SiO_2/MeOH: CH_3Cl = 3:7) to afford **3**. NMR peaks are assigned as follows. ^{1}H NMR (400 MHz, CDCl3, TMS): δ (ppm) 9.22-8.45 (6H), 4.79 (1H), 3.30-3.26 (1H), 2.0-1.8 (4H), 1.6-0.95(16H).

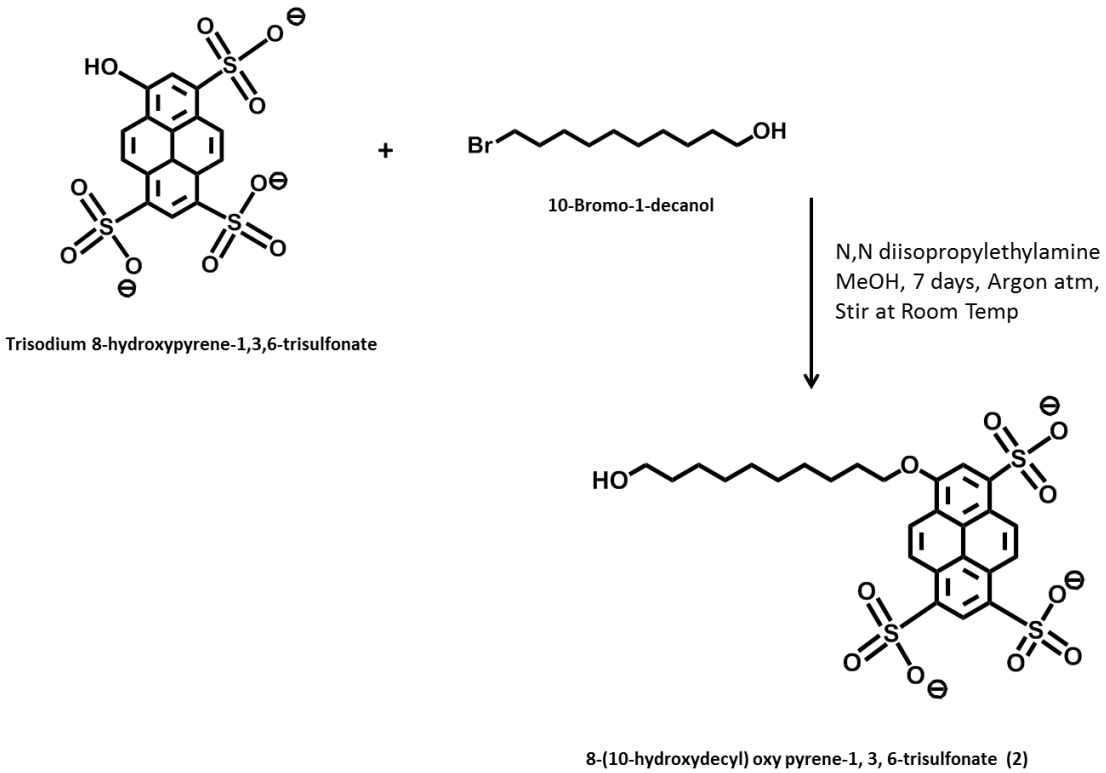

3.3.5 Synthesis of 8-oxydecylpyrene-1,3,6-trisulfonato lipoate (3):

1 mmol of lipoic acid was dissolved in 10 mL of anhydrous dichloromethane along with 1 mmol of DCC (N, N'-dicyclohexylcarbodiimide), 0.1 mmol of 4-DMAP (N, N-diisopropylethylamine), and 1 mmol of 8-((10-hydroxydecyl) oxy) pyrene-1,3,6-trisulfonate **(2)**. The mixture was stirred for 10 minutes at 0 ^{0}C under argon atmosphere. The stirring continued for 24 h at RT. The crude product was purified using column chromatography (SiO_2/MeOH: CH_3Cl = 7:3) to afford **3.** NMR peaks are assigned as follows. ^{1}H NMR (400 MHz, CDCl3, TMS): δ (ppm) 9.18-8.35 (6H), 4.5 (2H), 4.0 (2H), 3.2-2.8 (4H), 2.17 (1H), 2.0 (2H), 1.8-1.2 (20H).

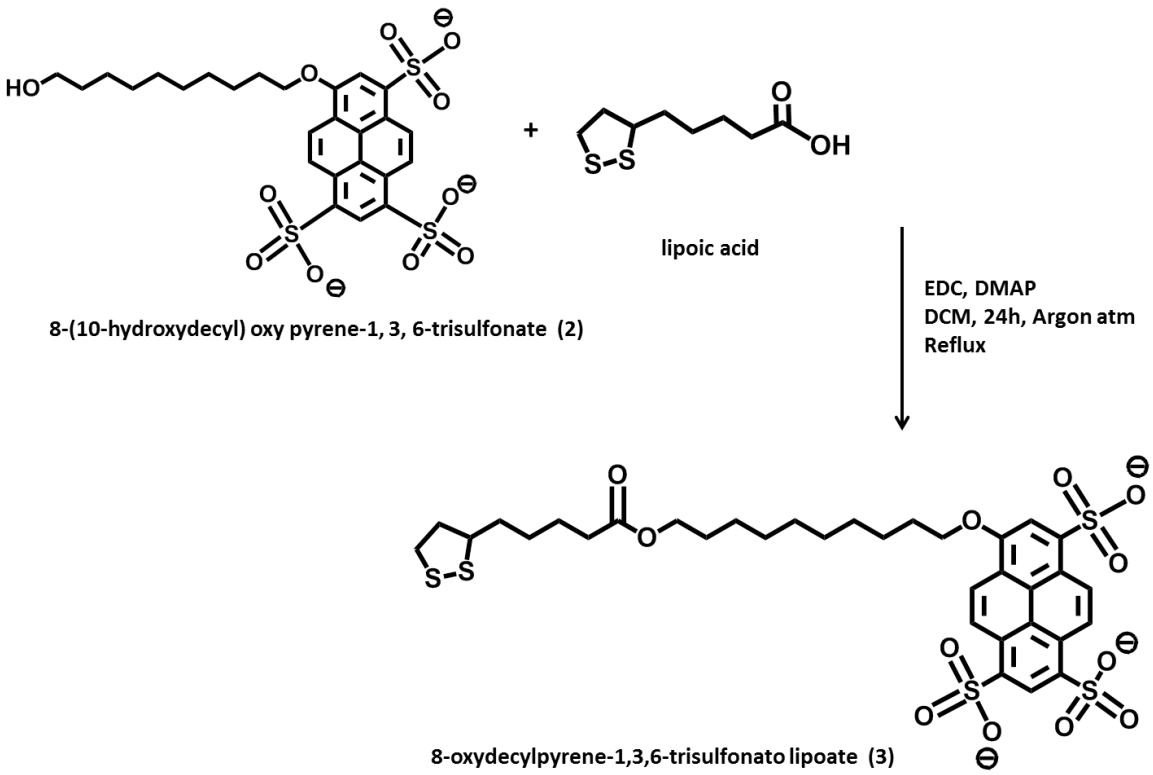

3.3.6 Synthesis of end-functional gold nanorods:

10 mL as synthesized gold nanorod solution was concentrated by centrifuging at 12000 rpm for 20 minutes. After discarding the supernatant, the precipitate was dispersed in 5 mL deionized water (concentration of gold nanorod solution is approximately 0.5 nM, calculated using molar absorption coefficient available from literature[25]). End-functional gold nanorods were prepared by mixing 1.5 mL of concentrated gold nanorod solution and 100 µL of 1 mM solution of respective donor or acceptor molecules. The mixture was kept stirring for 12 h. The gold nanorod solution was centrifuged and re-dispersed in 1.5 mL deionized water to remove unbound donor or acceptor molecules.

3.3.7 Solution state binding studies:

5 mL of 1 mM stock solutions of the viologen and pyranine ligands in water was prepared. 2 mL solutions containing 5 µM pyranine and required amount of viologen ligand

(1- 6 µM) were prepared. The fluorescence emissions of each sample were measured separately. Stern-volmer plot was constructed by plotting emission intensity versus concentration of the viologen.

3.3.8 Characterization:

TEM images were obtained using JEOL, JEM 3010 operated at 300 kV. UV-Vis spectra were recorded on a Perkin Elmer Lambda 900 UV-Vis-NIR spectrometer. Emission spectra were recorded on Perkin Elmer Ls 55 Luminescence Spectrometer. NMR spectra were obtained with a Bruker AVANCE 400 (400 MHz) Fourier transform NMR spectrometer. Zeta potential measurements were carried out using a NanoZS (Malvern UK) instrument.

3.4 Results and Discussion

Gold nanorods were synthesised according to a typical seed mediated method.[24] Figure-2a shows the TEM image of the as synthesised gold nanorods. The average length and width of the gold nanorods are found to be 35 nm and 10 nm respectively. Figure-2b shows the UV-vis absorption spectrum of the gold nanorods in water. Gold nanorods exhibit two distinct surface plasmon resonance (SPR) peaks located at 515 nm and 810 nm – corresponding to transverse and longitudinal plasmon resonance respectively. The position of the longitudinal plasmon resonance (LSPR) peak (815 nm) matches well with that of previously reported gold nanorods having aspect ratio 3.5.[25]

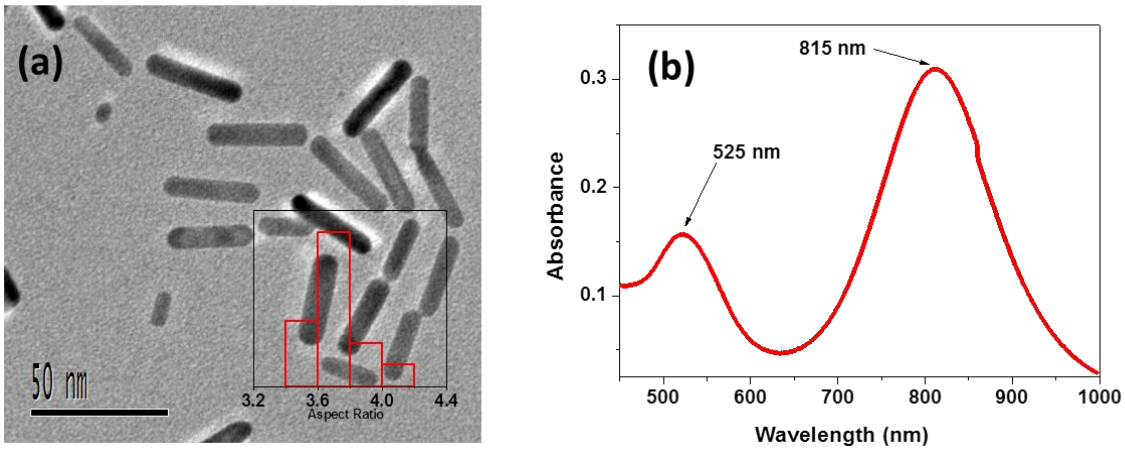

Figure-2: (a) TEM image of the as synthesized gold nanorods. (b) UV-vis absorption spectrum of gold nanorods in water.

To obtain end-to-end assembly of gold nanorods, it is necessary to have a strong charge transfer interaction between the donor and acceptor molecules. Association constant of charge transfer complex is a measure of the strength of charge transfer interaction.[26] Though the solution state association constant would be different from that in solid scaffolds, it can represent the extent of CT interactions between donor and acceptor. Solution state association constants for CT interaction of electron donor with viologen ligand were determined using fluorescence quenching experiments.[27]

Fluorescence quenching can occur through two mechanisms, namely – dynamic quenching and static quenching. In dynamic quenching, collision between the quencher and fluorophore occurs during the excitation lifetime of the fluorophore, whereas in static quenching, complexation occurs in the ground state between the quenching species and the fluorophore.[28] Association constant for the charge transfer interaction is equal to the rate constant of the static quenching[29], which can be calculated using Stern-Volmer equation as given below.

$$\frac{I_0}{I_Q} = 1 + K_s[Q]$$

where [Q] is the concentration of the quencher, I_0 is the measured fluorescence intensity without quencher, I_Q is the intensity with [Q] amount of quencher present.

Figure-3a shows the binding titration for the CT complex of pyranine **(3)** and viologen **(1)** in water. Figure-3b shows the Stern-Volmer plot for the pyranine-viologen complex. The solution state association constant for the pyranine-viologen CT complex is found to be 3.35×10^5 M^{-1}.

Figure-4a & b show the UV-vis absorption spectra of the pyranine- viologen complex in water. Appearance of a clear shoulder CT band (encircled in Figure-4a, enlarged in Figure-4b) from 420 nm – 500 nm show the formation of charge-transfer complex between pyranine and viologen.

To validate the proposed strategy for the end-to-end self-assembly of the gold nanorods, two sets of gold nanorod solutions were prepared - one with pyranine end-functionalized gold nanorods and the other with viologen end-functionalized gold nanorods. It is well documented that end-functionalization of the CTAB covered gold nanorods is possible, on account of strong preferential binding of CTAB molecules to the {100} facet of long face of gold nanorods. Since the binding of CTAB to the {111} facet at the curved ends of the gold nanorods is comparatively weaker, it is possible to specifically replace these CTAB molecules with thiolated ligand which have more affinity towards gold surface.[18]

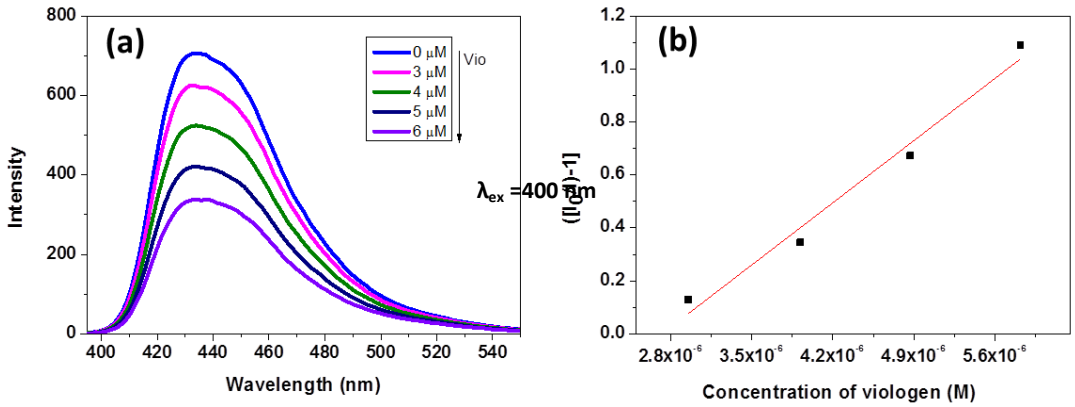

Figure-3: (a) Solution state binding titrations and, (b) Stern-Volmer plot for the CT association constant for pyranine-viologen CT complexation in water.

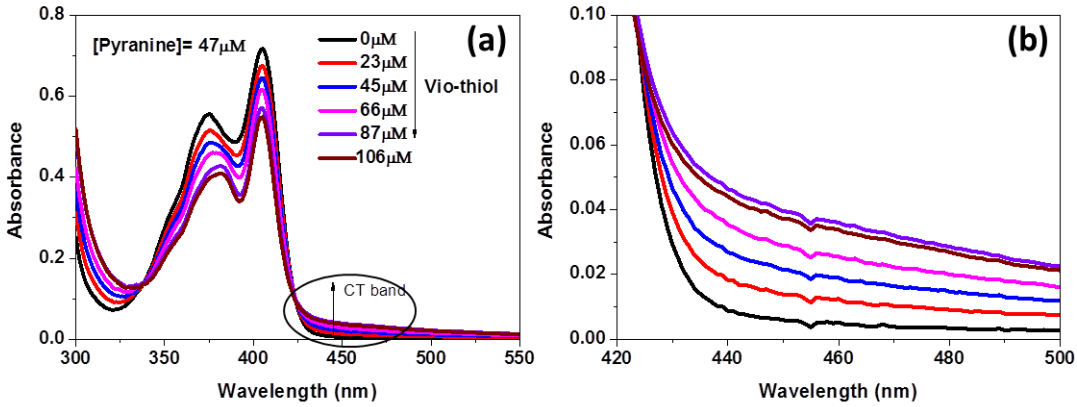

Figure-4: (a) UV-vis absorption spectra of the pyranine- viologen complex in water, (b) CT band of pyranine-viologen complex.

Figure-5a & b show the UV-vis absorption spectra of gold nanorods before and after viologen **(1)** and pyranine **(3)** ligands attachment respectively. For both the ligands, no change in LSPR peak width of gold nanorods was observed suggesting no undesired aggregation took place during the process of ligand binding. But a blue shift of LSPR about 20 nm was observed, which can be explained by the slight change in the length of the gold nanorods during the anchoring process.[30] Another important change is the upshift of

transverse plasmon (TSPR) peak at 524 nm upon ligand attachment. This can be explained by the spherical particle formation from the rods upon stirring.[31]

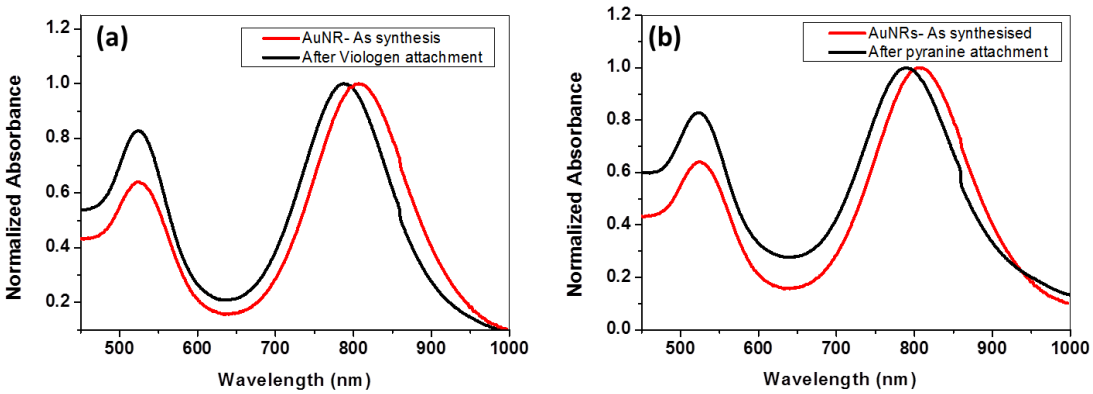

Figure-5: (a) Normalized UV-vis absorption spectra of gold nanorods before and after anchoring viologen ligand **(1)** (b) Normalized UV-vis absorption spectra of gold nanorods before and after pyranine ligand **(3)**.

To check the end-to-end assembly of the gold nanorods through pyranine-viologen CT interaction, two sets of gold nanorods- one with viologen end-functionalized and the other with pyranine end functionalized- were mixed in 1:1 proportion and the UV-vis absorption was monitored with time (Figure-6a). The intensity of the longitudinal plasmon peak (790 nm) reduces with time with simultaneous appearance of a new band at 950 nm. It is important to note the presence of a clear isosbestic point at 860 nm suggesting the presence of two types of gold nanorods. Though the reduction in the longitudinal plasmon is marginal, it nevertheless indicates the presence of two types of gold nanorods in the solution- isolated and assembled gold nanorods. The new band is appearing due the plasmon coupling of the individual nanorods assembled in end-to-end fashion.[32] Figure-6b represents the variation of absorption at 790 nm and 950 nm during the process of self-assembly.

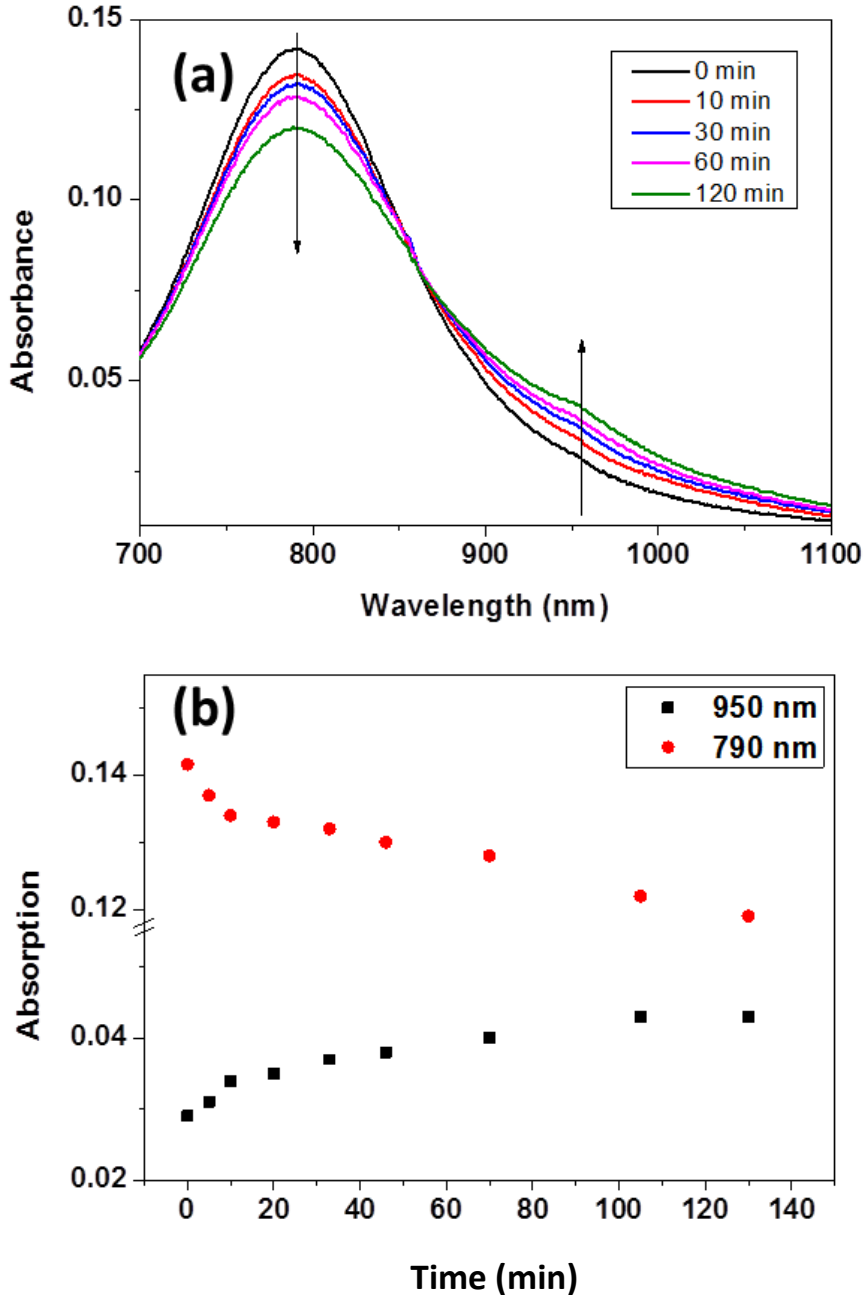

Figure-6: (a) UV-Vis absorption spectra of the assembly mixture at different time intervals. (b) Variation of the absorption at 790 nm and 950 nm with time.

A blank experiment was carried out to make sure CT interaction is the cause for the plasmonic coupling and to rule out any possible interference. The time dependent variation of absorption for unmodified gold nanorods is determined (Figure-7). Spectra remained same with time, ruling out any possible assembly in the system.

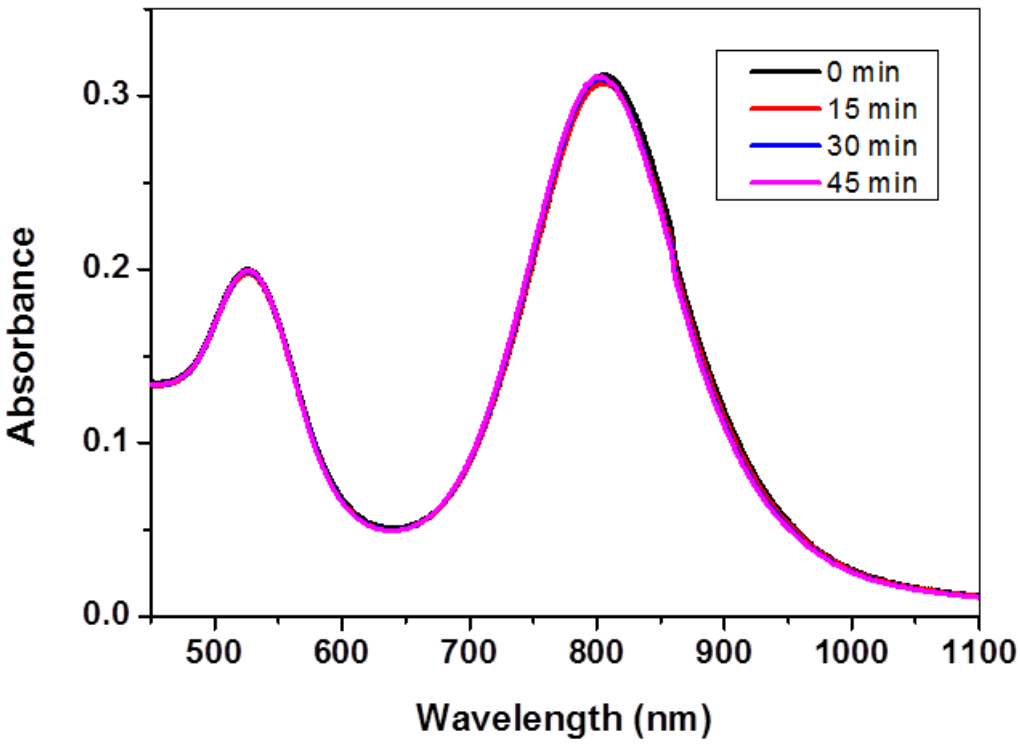

Figure-7: UV-Vis absorption spectra of unmodified gold nanorods at different intervals.

In order to rule out the possibility of any assembly due to electrostatic attraction between negatively charged pyranine and positively charged CTAB covered gold nanorods, another control experiment was also carried out by mixing pyranine anchored gold nanorods and CTAB covered gold nanorods. Figure-8 shows the UV-vis absorption spectra of the mixture containing the pyranine connected gold nanorods and CTAB covered gold nanorods. Spectra remain more or less same with time, indicating no assembly of gold nanorods in the absence of CT interaction. Thus it is undoubtedly clear that the CT interaction is the key factor for the assembly of the gold nanorods.

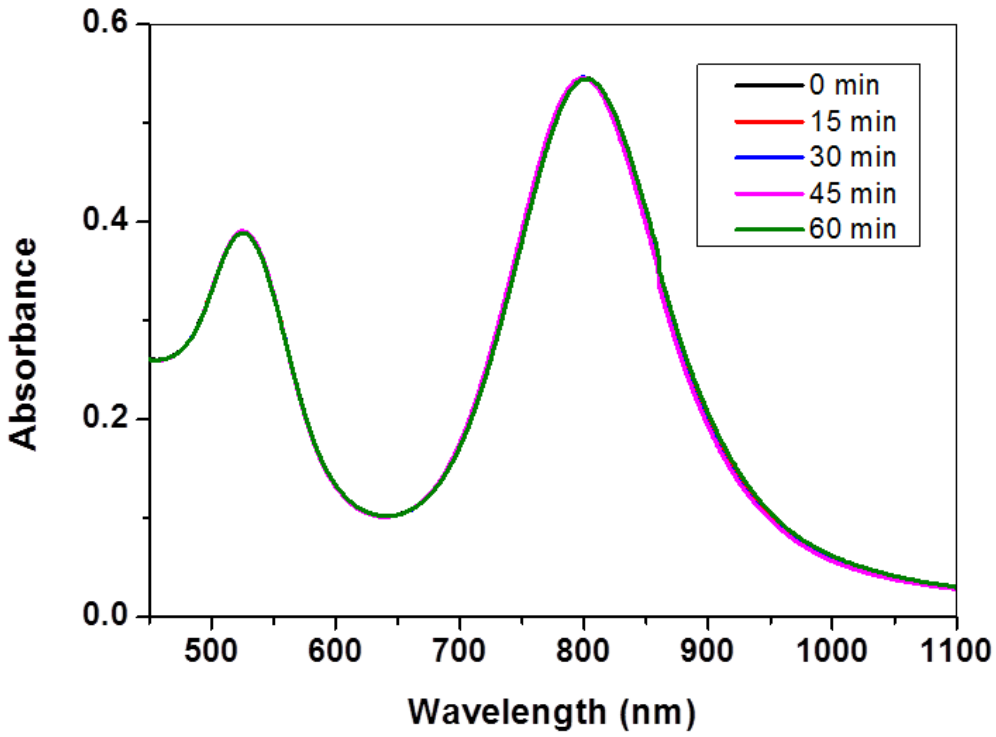

Figure-8: UV-Vis absorption spectra of the mixture containing pyranine anchored gold nanorods and CTAB coated gold nanorods at different intervals.

The reversibility of the pyranine-viologen complexation with respect to the reduction and oxidation is studied in solution. Sodium dithionate was used as the reducing agent to reduce viologen di-cation to viologen radical cation which cannot form CT complex with pyranine. K_3 [$Fe(CN)_6$] was used as the oxidizing agent to bring back reduced viologen to viologen di-cation. Figure-9 shows the fluorescence intensity variation upon addition of reducing and oxidizing agents. The emission intensity of the pyranine-viologen complex was enhanced by adding reducing agent, which indicates the breakage of CT between ligands. Further addition of oxidizing agent quench the emission shows that CT complex forms again. Reversibility was found up to three cycles of oxidation and reduction of viologen moieties.

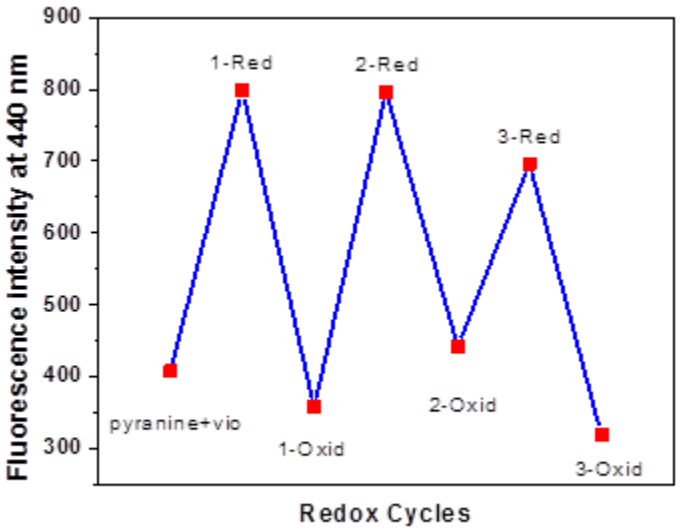

Figure-9: Emission intensity variation upon addition of reducing and oxidizing agents. This shows the reversibility of CT complex in solution.

3.5 Conclusion

We have demonstrated a new strategy for the end-to-end assembly of the gold nanorods involving the charge transfer interaction between the donor and acceptor molecules. Two sets of gold nanorods were prepared- one with donor molecules and other with acceptor molecules tethered to the end. The self-assembly of the gold nanorods is established by mixing the both sets of gold nanorod solutions. The redox reversibility of CT association of the donor and acceptor pair was studied.

3.6 Future Prospects:

The ultimate goal of this study is yet to be achieved with hetero metallic nanorods of *AB* type self-assembly, similar to alternative copolymerization. *AB* type of plasmonic copolymerization has not been well addressed in the literature. We propose CT assisted strategy for copolymerization of the hetero metal nanorods as depicted in Figure-10, owing to

the specificity of CT interaction between donor and acceptor to obtain precise control over alternative assembly.

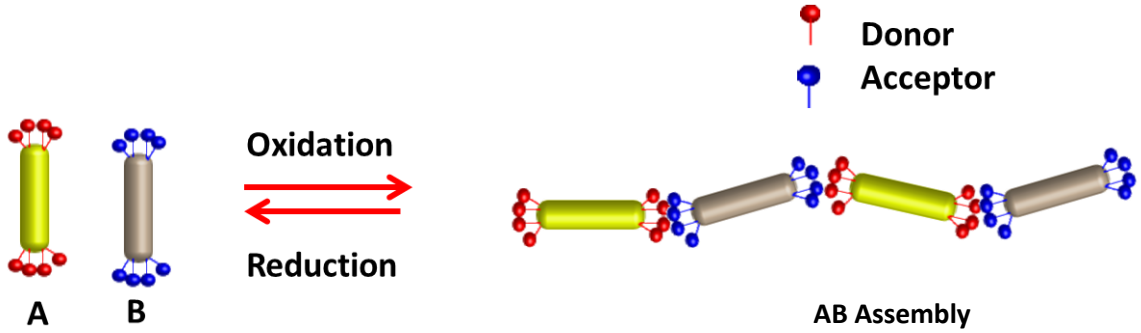

Figure-10: Schematic representation of the future extension of strategy presented in this chapter.

3.7 References:

1 Rao, C. N. R., Kulkarni, G. U., Thomas, P. J. & Edwards, P. P. Metal nanoparticles and their assemblies. *Chem. Soc. Rev.* **29**, 27-35, (2000).

2 Schmid, G. *Encyclopedia of Inorganic Chemistry* (John Wiley & Sons, Ltd, 2006).

3 Warner, M. G. & Hutchison, J. E. Linear assemblies of nanoparticles electrostatically organized on DNA scaffolds. *Nat Mater* **2**, 272-277, (2003).

4 Kim, B., Tripp, S. L. & Wei, A. Self-Organization of Large Gold Nanoparticle Arrays. *J. Am. Chem. Soc.* **123**, 7955-7956, (2001).

5 Liz-Marzán, L. M. Tailoring Surface Plasmons through the Morphology and Assembly of Metal Nanoparticles. *Langmuir* **22**, 32-41, (2005).

6 Nie, Z., Petukhova, A. & Kumacheva, E. Properties and emerging applications of self-assembled structures made from inorganic nanoparticles. *Nat Nano* **5**, 15-25, (2010).

7 Tang, Z. & Kotov, N. A. One-Dimensional Assemblies of Nanoparticles: Preparation, Properties, and Promise. *Adv. Mater.* **17**, 951-962, (2005).

8 Slaughter, L. S., Willingham, B. A., Chang, W.-S., Chester, M. H., Ogden, N. & Link, S. Toward Plasmonic Polymers. *Nano Lett.* **12**, 3967-3972, (2012).

9 Xu, L., Kuang, H., Wang, L. & Xu, C. Gold nanorod ensembles as artificial molecules for applications in sensors. *J. Mater. Chem.* **21**, 16759-16782, (2011).

10 Ozbay, E. Plasmonics: Merging Photonics and Electronics at Nanoscale Dimensions. *Science* **311**, 189-193, (2006).

11 Maier, S. A., Kik, P. G., Atwater, H. A., Meltzer, S., Harel, E., Koel, B. E. & Requicha, A. A. G. Local detection of electromagnetic energy transport below the diffraction limit in metal nanoparticle plasmon waveguides. *Nat Mater* **2**, 229-232, (2003).

12 Lee, A., Andrade, G. F. S., Ahmed, A., Souza, M. L., Coombs, N., Tumarkin, E., Liu, K., Gordon, R., Brolo, A. G. & Kumacheva, E. Probing Dynamic Generation of Hot-

Spots in Self-Assembled Chains of Gold Nanorods by Surface-Enhanced Raman Scattering. *J. Am. Chem. Soc.* **133**, 7563-7570, (2011).

13 Nie, Z., Fava, D., Kumacheva, E., Zou, S., Walker, G. C. & Rubinstein, M. Self-assembly of metal-polymer analogues of amphiphilic triblock copolymers. *Nat Mater* **6**, 609-614, (2007).

14 Liz-Marzán, L. M., Giersig, M. & Mulvaney, P. Synthesis of Nanosized Gold−Silica Core−Shell Particles. *Langmuir* **12**, 4329-4335, (1996).

15 Jain, P. K., Eustis, S. & El-Sayed, M. A. Plasmon Coupling in Nanorod Assemblies: Optical Absorption, Discrete Dipole Approximation Simulation, and Exciton-Coupling Model. *J. Phys. Chem. B* **110**, 18243-18253, (2006).

16 Lukach, A., Liu, K., Therien-Aubin, H. & Kumacheva, E. Controlling the Degree of Polymerization, Bond Lengths, and Bond Angles of Plasmonic Polymers. *J. Am. Chem. Soc.* **134**, 18853-18859, (2012).

17 Grubbs, R. B. Nanoparticle assembly: Solvent-tuned structures. *Nat Mater* **6**, 553-555, (2007).

18 Caswell, K. K., Wilson, J. N., Bunz, U. H. F. & Murphy, C. J. Preferential End-to-End Assembly of Gold Nanorods by Biotin−Streptavidin Connectors. *J. Am. Chem. Soc.* **125**, 13914-13915, (2003).

19 Wang, Y., Li, Y. F., Wang, J., Sang, Y. & Huang, C. Z. End-to-end assembly of gold nanorods by means of oligonucleotide-mercury(ii) molecular recognition. *Chem. Commun.* **46**, 1332-1334, (2010).

20 Huang, H., Liu, X., Hu, T. & Chu, P. K. Ultra-sensitive detection of cysteine by gold nanorod assembly. *Biosens. Bioelectron.* **25**, 2078-2083, (2010).

21 Sudeep, P. K., Joseph, S. T. S. & Thomas, K. G. Selective Detection of Cysteine and Glutathione Using Gold Nanorods. *J. Am. Chem. Soc.* **127**, 6516-6517, (2005).

22 Yonemoto, E. H., Saupe, G. B., Schmehl, R. H., Hubig, S. M., Riley, R. L., Iverson, B. L. & Mallouk, T. E. Electron-Transfer Reactions of Ruthenium Trisbipyridyl-

Viologen Donor-Acceptor Molecules: Comparison of the Distance Dependence of Electron Transfer-Rates in the Normal and Marcus Inverted Regions. *J. Am. Chem. Soc.* **116**, 4786-4795, (1994).

23 Kumar, B. V. V. S. P., Rao, K. V., Soumya, T., George, S. J. & Eswaramoorthy, M. Adaptive Pores: Charge Transfer Modules as Supramolecular Handles for Reversible Pore Engineering of Mesoporous Silica. *J. Am. Chem. Soc.* **135**, 10902-10905, (2013).

24 Gorelikov, I. & Matsuura, N. Single-Step Coating of Mesoporous Silica on Cetyltrimethyl Ammonium Bromide-Capped Nanoparticles. *Nano Lett.* **8**, 369-373, (2007).

25 Orendorff, C. J. & Murphy, C. J. Quantitation of Metal Content in the Silver-Assisted Growth of Gold Nanorods. *J. Phys. Chem. B* **110**, 3990-3994, (2006).

26 Gauthier, T. D., Shane, E. C., Guerin, W. F., Seitz, W. R. & Grant, C. L. Fluorescence quenching method for determining equilibrium constants for polycyclic aromatic hydrocarbons binding to dissolved humic materials. *Environmental Science & Technology* **20**, 1162-1166, (1986).

27 Keizer, J. Nonlinear fluorescence quenching and the origin of positive curvature in Stern-Volmer plots. *J. Am. Chem. Soc.* **105**, 1494-1498, (1983).

28 Kumar Behera, P. & Kumar Mishra, A. Static and dynamic model for 1-naphthol fluorescence quenching by carbon tetrachloride in dioxane—acetonitrile mixtures. *Journal of Photochemistry and Photobiology A: Chemistry* **71**, 115-118, (1993).

29 de Borba, E. B., Amaral, C. L. C., Politi, M. J., Villalobos, R. & Baptista, M. S. Photophysical and Photochemical Properties of Pyranine/Methyl Viologen Complexes in Solution and in Supramolecular Aggregates: A Switchable Complex. *Langmuir* **16**, 5900-5907, (2000).

30 Li, F.-M., Liu, J.-M., Wang, X.-X., Lin, L.-P., Cai, W.-L., Lin, X., Zeng, Y.-N., Li, Z.-M. & Lin, S.-Q. Non-aggregation based label free colorimetric sensor for the

detection of Cr (VI) based on selective etching of gold nanorods. *Sensors and Actuators B: Chemical* **155**, 817-822, (2011).

31 Link, S., Burda, C., Nikoobakht, B. & El-Sayed, M. A. How long does it take to melt a gold nanorod?: A femtosecond pump–probe absorption spectroscopic study. *Chem. Phys. Lett.* **315**, 12-18, (1999).

32 Liu, K., Ahmed, A., Chung, S., Sugikawa, K., Wu, G., Nie, Z., Gordon, R. & Kumacheva, E. In Situ Plasmonic Counter for Polymerization of Chains of Gold Nanorods in Solution. *ACS Nano* **7**, 5901-5910, (2013).